PORTLAND LIMESTONE CEMENT WITH FLY ASH: FREEZE-THAW DURABILITY AND MICROSTRUCTURE STUDIES

A Thesis
Submitted to the Graduate Faculty
of the
North Dakota State University
of Agriculture and Applied Science

By

Prokshit Abhinandan Angadi

In Partial Fulfillment of the Requirements
for the Degree of
MASTER OF SCIENCE

Major Department:
Construction Management and Engineering

November 2018

Fargo, North Dakota

North Dakota State University
Graduate School

Title

Portland Limestone Cement with Fly Ash: Freeze-Thaw Durability and Microstructure Studies.

By

Prokshit Abhinandan Angadi

The Supervisory Committee certifies that this ***disquisition*** complies with North Dakota State University's regulations and meets the accepted standards for the degree of

MASTER OF SCIENCE

SUPERVISORY COMMITTEE:

Dr. Todd Sirotiak
Chair

Dr. Matthew Stone

Dr. Ying Huang

Approved:

November 16,2018
Date

Dr. Jerry Gao
Department Chair

ABSTRACT

In this study, the freeze-thaw performance and other engineering properties of different cementitious mixtures containing Type I/II portland cement, Type IL (10) portland Limestone cement (PLC) and Coarse Ground cement (CG-P) with or without partial replacement of fly ash (Class F) were examined. The goal was to develop a concrete mixture with better or similar freeze-thaw durability without adversely affecting other engineering properties of concrete.

Crucial engineering properties reviewed include compressive strength, splitting tensile strength, workability, the degree of hydration, setting time, shrinkage and resistivity. The study was divided into two parts, one consisting of mechanical testing of engineering properties including the freeze-thaw test. The second part consisted of microstructure study which involved detection and quantification of micro-cracks/defects using μ-CT and fluorescence microscopy. The results showed that the portland limestone cement in combination with fly ash demonstrated better or similar durability in comparison to the conventional portland cement concrete mixtures.

ACKNOWLEDGMENTS

I would like to start by thanking my parents, Mr. Abhinandan Angadi and Ms. Vatsala Angadi for their blessing and extraordinary support. Likewise, I would like to thank my advisor Dr. Todd Sirotiak. His vast knowledge and experience has been a major boon and played an irreplaceable role towards completing my degree.

I thank my committee members Dr. Matthew Stone and Dr. Ying Huang for providing me valuable remarks, guidance, and support throughout my research and graduate program.

I extend my gratitude to Dr. Achintyamugdha Sharma for his exceptional direction and in-depth technical guidance. I would also like to thank my fiancé Priyanka Pujar for her incredible support and perseverance.

I would like to thank my fellow NDSU graduate student Asif Abubakar for his generous support during this study. I profusely thank Ann Denney and Ingrid Skarski for providing me administrative and moral support and making my graduate program a fulfilling journey.

I would like to thank North Dakota Department of Commerce for supporting this study under the N.D Venture Grant. I also thank and acknowledge Mr. Henry Hauge for his generous support in the form of materials for this study and his insight.

DEDICATION

I dedicate this thesis to my Parents, who have sacrificed so much for my sake. They taught me to tackle any and all challenges in my life with a focus on the positive side of things and to make sure to always help others at every chance you get and lastly to never ever lose hope.

TABLE OF CONTENTS

LIST OF TABLES

LIST OF FIGURES

LIST OF ABBREVIATIONS

OPC.....Ordinary Portland Cement

PLC .....Portland Limestone Cement

CGP.....Coarse Ground Cement

CG-P .....Coarse Ground Cement

µ-CT.....Microcomputed Tomography

FM.....Fluorescence Microscopy

FA .....Fly ash

bg. .....Background

LIST OF SYMBOLS

μ ....Micro

1. INTRODUCTION AND LITERATURE REVIEW

The extensive use of concrete as a construction material is due to its durability and the ability to be cast into any shape in its plastic state. However, concrete, like any other material, has its limitations. This study focuses on one of those limitations namely the durability of the concrete. The durability of the concrete is its ability to withstand weather effects, chemical attacks and physical effects like abrasion and shocks without losing its engineering properties. There are two main potentially destructive factors that affect the concrete durability. The first factor is the effect of ingress of deleterious ions. Another critical limitation of concrete is its loss of durability when subjected to freezing and thawing.

When water inside concrete pores start to freeze, the frozen water expands and increases in volume, thereby creating hydraulic pressure. This phenomenon leads to dilation and rupturing of capillary pores. The magnitude of this hydraulic pressure at a particular location inside a concrete specimen depends upon its distance from the surface of the specimen, the permeability of the material and the rate of ice formation. The cumulative effect of freezing and thawing leads to deterioration of cement paste and aggregate, eventually causing expansion, scaling and cracking of the concrete [1,2]. It has been reported that the formation of ice crystallization pressures within pores inside cement paste causes internal-frost damage to the cement paste [3].

It has also been well documented that adding an air-entraining agent during the mixing of concrete can potentially enhance its freeze-thaw resistance [2,4–7]. This is due to entrained air voids, which are larger than capillary pores. These pores relieve hydraulic pressure from the freezing of water in the capillary pores.

Another shortcoming of portland cement is the emission of carbon dioxide (CO_2) into the atmosphere during its manufacturing process. CO_2 is emitted during the manufacture of ordinary

portland cement because of two significant processes, clinker formation and the use of fossil fuels (as identified by previous researchers). This emission of CO_2 may be reduced by partial replacement of portland cement with other supplementary cementitious materials like fly ash and slag. The inclusion of a high volume of fly ash may help significantly reduce CO_2 emissions. One relatively less researched cementitious material with a partial replacement of portland cement clinker, interground with limestone, is portland limestone cement (PLC).

1.1. Portland Limestone Cement (PLC)

Utilization of PLC results in a more environmentally sustainable concrete, with a reduced carbon footprint and lowered embodied production energy when compared to ordinary portland cement (OPC) [8]. Provision for PLC's inclusion of 5-15% limestone was added to ASTM C595 and AASHTO M 240 specifications for blended cement in 2012 [9].

PLC is produced by intergrinding cement clinkers with limestone during the manufacturing process. As limestone is softer than clinker [10], the same grinding energy results in the formation of smaller particles of limestone, in comparison to those of portland cement. This results in a better particle size distribution (PSD), or particle packing [10–13]. Rather than behaving as an inert filler, limestone helps accelerate the hydration process by multiple mechanisms. The presence of limestone in PLC results in more nucleation sites, acting as a nucleus for the growth of hydration products [14]. Limestone also increases the hydration rate of calcium silicates at early ages [15], as it reacts with aluminate phases to form carbo-aluminate hydrates [15,16]. These carbo-aluminate hydrates are more stable than other hydration products [17] and fill interfacial transition zones (ITZ) between cement paste and aggregates, improving the microstructure of the mixture [18]. They are formed from the first day of mixing and may remain present even after 28 days [19].

The combined effect of these mechanisms is the higher early strength of concrete containing PLC as compared to that containing OPC. Interestingly, Bonavetti et al. [16] suggested that when fly ash is added to concrete containing PLC, the additional alumina provided by fly ash in the mixture could extend the reaction between limestone and aluminate phases and produce more carbo-aluminates. Meanwhile, another study [12] reported that when PLC is partially replaced with fly ash, the resultant concrete exhibited a reduction in permeable voids and chloride ion diffusion coefficients in comparison to concrete containing OPC and fly ash. Overall results suggested better performance of PLC containing fly ash.

Various studies have debated the limestone content in PLC and its effects on the mixture properties in comparison to ordinary portland cement (OPC). A study [20] in 2009, considered (0,5,10,15 and 20% limestone) cement mixtures and found PLC with 5% and 10% limestone demonstrated similar properties to OPC, while limestone of 15% and 20% exhibited poorer properties. Hence the authors suggested 10 - 15% as the optimum amount of limestone. Another study [21] showed similar results and recommended up to 15% limestone replacement to obtain similar performance as OPC mixtures. The results of [22,23] also showed that PLC with up to 10% limestone has no adverse effects on the mechanical properties of the concrete.

1.2. Fly Ash

Using optimal type and amount of supplementary cementitious materials (SCMs) like fly ash is considered to be a cost-effective approach to enhance the durability of concrete [3]. High volumes of ASTM Class F fly ash-based mixtures have exhibited satisfactory freeze-thaw durability results [22].

When fly ash is added to the mixture, the fly ash particles are attracted and absorbed to the oppositely charged surfaces of the cement particles, preventing flocculation. This effective

dispersion helps to trap large amounts of water, thus reducing water demand. Fly ash particles have a spherical shape and smooth surface which helps to reduce interparticle friction and add a lubricating effect. They are also known to improve particle packaging effect, acting as an exceptional filler for the void space within the aggregate mixture. Fly ash is a low density, high volume per unit mass which makes it even more efficient in filling void space when compared to portland cement. Fly ash also helps drive the pozzolanic reaction which converts the hydration product calcium hydroxide ($Ca(OH)_2$) to additional calcium silicate hydrate gel (C-S-H) [24,25], leading to higher long-term strength gain.

1.3. Coarse Ground Portland Cement

In case of coarse ground cement type, the Blaine Fineness is marginally lower than OPC. Coarser cements reportedly produce less heat during hydration and also experience lower shrinkage compared to finer cements like OPC [26]. According to the Young-Laplace relationship, capillary stress is inversely proportional to the radius of the emptying pore. This means that with larger pores (greater than 50nm), coarser cement (CG-P) concrete mixtures could lead to low capillary stress and result in a reduction in shrinkage of the mixture [27]. The lower shrinkage property is estimated to lead to the lesser crack formation and higher water tightness, with potentially better freeze-thaw resistance.

1.4. Cementitious Combinations

In this study, five different cementitious combinations were investigated. These combinations were produced by three different types of cement: Type I/II portland cement (TI/II), Type IL portland limestone cement (TIL) and Coarse ground portland cement (CG-P) with or without partial replacement with Class F Fly ash (FF) at varying dosages (%).

1.5. Research Needs

Although there is plenty of research available which demonstrates portland limestone cement (PLC) can help to prevent the reduction of early age strength due to the addition of fly ash, the durability aspect of PLC based concrete has not been researched to the same degree [28,29]. Some studies have also suggested that more research is needed to evaluate the degree of permeability of the PLC and fly ash mixtures [30]. Although, there have been some European freeze-thaw studies done in the past, they are based upon non-air-entrained concrete mixtures [21,29,31–33]. A study from Canada [34] showed that the combination of portland limestone cement (10-15% limestone replacement) and Slag (30% replacement) demonstrated no negative effect on freeze-thaw resistance. They also noted that in lower temperatures, high-C_3A PLC is more prone to formation of thaumasite. However, results showed that combining slag or similar pozzolans like fly ash has shown to improve sulfate resistance and prevent thaumasite at low temperatures.

This study aims to dwell a little deeper into studying the durability properties like mainly freeze-thaw of the portland limestone cement concrete with and without fly ash replacement in comparison to ordinary portland cement concrete mixtures.

As this study was partly funded by the local state, North Dakota Department of Commerce Venture program, the local state codes and standards were adhered to for this study.

The North Dakota Department of Transportation mix design allows up to 29% replacement of portland cement with supplementary cementitious materials in concrete mixtures [35]. In addition, 37% fly ash replacement was chosen on the higher end of the replacement percentage; this specific content has been used in mass concreting purposes like parking lots in the state. These

replacement percentages mimic the recommended percentages utilized by the industry ready mix suppliers in the area

1.6. Goal and Objectives

Figure 1 provides a brief overview of the overall research methodology. The primary goal of this study was to investigate a durable concrete mixture by using Type IL (10) portland limestone cement (10% of portland cement clinker is replaced with limestone) with/without fly ash. Subsequent to this process, the mix would be subjected to rigorous testing methods to determine if the newly designed mix might be equivalent or better than OPC. Comparisons were made with a standard cementitious combination currently used for pavements and bridge decks by the North Dakota Department of Transportation (NDDOT). Additionally, other durability indicators such as electrical resistivity and drying shrinkage, and other vital engineering properties of concrete in its plastic and hardened states such as, workability, air content (%), the degree of hydration, compressive and splitting tensile strengths were also investigated. Furthermore, some of the microstructure properties of cement paste consisting of the above-mentioned cementitious

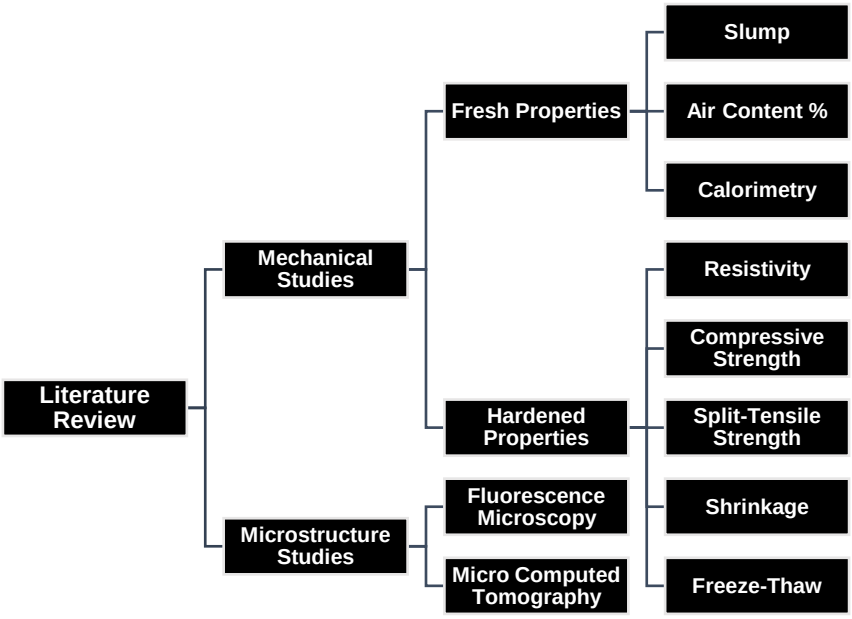

Figure 1: Research flowchart

combinations such as maximum porosity, void size distribution and microcracking (defects) tendency were also investigated. One of the major goals of this study was to investigate the potential relationships between microstructure properties, as mentioned above, of paste samples subjected to drying conditions under restraint and bulk properties of concrete.

1.7. Microstructure Study

Concrete is known to be highly moldable in its plastic state. When the cement reacts with the water, it begins to act as a binding agent within the mixture. Sometimes during this reaction, the water remains unreacted. The unreacted water gets evaporated leaving behind voids. These voids have the ability to influence the strength and impermeability of the mixture [36].

The surface of an exposed specimen experiences a higher degree of drying in comparison to the inner layers which causes the formation of a steep moisture gradient, leading to tensile stress which is parallel to the exposed drying surface[37,38]. Since the shrinking tendency of the cement paste (weak in tension) is higher than the aggregates, the bond between the paste and aggregate gets unbounded creating intergranular/radial microcracks (0.25-50μ) [37].

The porosity and permeability of the concrete are higher on the surface and decreases as the depth from the surface increases [39]. Hence, the upper regions exhibit higher porosity and have a higher tendency of developing micro-cracks. These micro-cracks may provide entry to chemical ions like chloride and sulfate ions, which are highly detrimental to the mixture and can react with hydration products to form expansive compounds which ultimately reduce the durability of the mixture. Permeability is dependent upon the capillary pore structure and the interconnectivity of these capillary pores. Higher porosity also has negative effects like making the steel reinforcement more susceptible to corrosion and making the concrete prone to freeze-thaw failures such as scaling [40–42]. The properties of the pores like pore size, distribution and

interconnectivity have an effect on the overall porosity [29,42]. Since the micro-pores/cracks/defects mostly originate in the paste, isolating the cement paste from the concrete mixtures and studying them might prove to be insightful.

The ASTM C1581 [43] ring test is commonly used to measure strain produced in the sample due to drying shrinkage. From a microscopy perspective, there are standards denoting petrographic analysis of concrete samples like ASTM C856 [44] but, they do not have a standard method to quantify or detect the micro-cracks due to drying shrinkage. Microscopy techniques such as optical microscopy and scanning electron microscopy (SEM) have been used by previous researchers to study the microstructure of the concrete and cement samples. Although one can observe the hydration products and the surface structure [45–47] using them, they tend to be very expensive and highly time-consuming. Prior researchers have also tried using fluorescence microscopy and digital image processing (DIP) to detect micro-cracks [48].

Researchers [49,50] have used fluorescence microscopy to study the air void system in concrete samples. The process followed consisted of concrete specimens which were dried to constant weight and then were vacuum impregnated by a low viscosity epoxy containing fluorescence dye. The vacuum impregnated sample was then placed inside a pressurized chamber to ensure proper epoxy penetration [50]. Later the specimens were grounded and polished in sequential stages into thin slices. The air void boundaries are preserved against crumbling during grinding and polishing process due to the hardened epoxy, while the fluorescence dye aids in highlighting of the air voids. The specimens which are polished concrete blocks, were examined at 40x magnification using a petrographic microscope with a set up capable of analyzing air voids as small as 10μm in diameter [49]. Fluorescence microscopy is used for detection and quantification of micro-cracks and explained further in section 2.3.2.

For micro-computed tomography or μ-CT is 3D x-ray imaging, the same system used in the medical field. μ-CT can be used to inspect objects micro-structure non-destructively. Unlike fluorescence microscopy method, μ-CT does not require any specimen conditioning like staining and thin slicing. A single scan is adequate to obtain a complete internal 3D structure at a high resolution, without destroying the specimen which can then be used for other micro-studies. Other methods of determining the porosity of cement composites include Mercury intrusion porosimetry (MIP), Alternating current impedance spectroscopy (ACIS), Nuclear Magnetic Resonance Imaging(MRI), helium inflow, image analysis, water absorption, gas adsorption, solvent replacement [51]. Even though non-destructive methods of testing have shown to be more effective in comparison to destructive methods, MIP and water absorption are commonly used methods which are effective destructive methods chosen to determine the total void ratio and defects [52–54].

The study proposed a method in which the paste specimen of cementitious combinations were studied under different microscopy techniques like micro-computed tomography (μ-CT) and Fluorescence Microscopy (FM).

Thus, a workflow consisting of different methods for investigating the microstructure of the cement paste specimens of the selected cementitious combination was developed. The goal was to get an understanding of the nature of the paste specimen at the microscopic level. The defects (%), porosity and void size distribution results obtained through these methods could be used to correlate with the engineering properties of the mixture.

2. MATERIALS AND METHODS

In this study, three different cement types, Type I/II cement, The Type IL, also referred as PLC cement with 10% limestone replacement, and coarse ground cement were investigated.

For supplementary cementitious materials (SCMs), Class F Fly ash was used. Two replacement levels of portland cement with fly ash, 29% and 37%.

Tables 1 and 2 show the various chemical and physical properties of the selected cement types and fly-ash respectively. A ¾ inch (nominal aggregate size) glacial till was used as coarse aggregate and locally available sand was used as fine aggregate.

An organic acid-based air entraining agent and a polycarboxylate based Type F high range water reducer were used. The admixture dosages and water to cementitious materials ratios (w/cm) were driven by considering mixture designs utilized by a local ready-mix concrete producer.

Table 1: Chemical and physical properties of cements selected

Item	**Coarse Ground Cement***	**Type I/II Cement***	**Type IL Cement****
SiO_2 (%)	21.07	20.31	-
Al_2O_3 (%)	4.25	3.79	-
Fe_2O_3 (%)	3.13	3.22	-
CaO (%)	65.00	64.29	-
MgO (%)	0.97	3.38	0.90
SO_3 (%)	2.88	2.26	3.10
Loss on ignition (%)	0.75	2.73	4.80
Na_2O (%)	0.14	0.09	-
K_2O (%)	0.58	0.20	-
Insoluble Residue (%)	0.21	0.37	0.40
CO_2 (%)	-	1.85	-
Limestone (%)	-	4.7	10.0
$CaCO_3$ in limestone (%)	-	90.16	96.20
C_3S (%)	61.62	60.00	-
C_2S (%)	12.44	11.00	-
C_3A (%)	5.83	4.00	7.00
C_4AF (%)	9.3	10.00	-
Equivalent alkalis (%)	0.52	0.23	-
Blaine Fineness (m^2/kg) ***	316.94	393.00	382.00

*Limits specified in ASTM C150
**Limits specified in ASTM C595
***Physical property

Table 2: Chemical and physical properties of fly ash used

Item	**Class F Fly Ash***
SiO_2 (%)	51.65
Al_2O_3 (%)	16.29
Fe_2O_3 (%)	5.63
SiO_2+Al_2O_3+Fe_2O_3	73.57
SO_3 (%)	0.67
CaO (%)	13.00
MgO (%)	4.26
Na_2O (%)	3.23
K_2O (%)	2.45
Equivalent alkalis (%)	1.63
Loss on Ignition (%)	0.10
Fineness (+325 Mesh) (%) **	21.29

*Limits specified in ASTM C618
**Physical property

2.1. Mixture Proportions

Table 3 shows mixture proportions for the concrete mixtures. The concrete mixtures that were selected for this study were Type I/II cement with 29% Class F fly ash replacement (TI/II-FF 29%), Type IL cement with no SCM (TIL-P), Type IL cement with 29% Class F fly ash replacement (TIL-FF 29%), Type IL cement with no SCM (TIL-P), Type IL cement with 37% Class F fly ash replacement (TIL-FF 37%), and coarse ground cement with no SCM (CG-P).

The water-cement ratio was kept at a constant of 0.43 (ASTM Code) for all mixtures. The binder content was fixed at 564 (lb./yd^3). The binder to fine aggregates to coarse aggregates weight ratio was set to 1:2.38:3.17.

Table 3: Mixture proportions for the study.

No.	Mix Code	Cement (pcy)	FA (pcy)	Water (pcy)	WR (oz/cwt)	AEA (oz/cwt)	Fine Agg. (pcy)	Coarse Agg. (pcy)
1	TI/II FF 29%	400	164	242	1.25	0.6	1340	1790
2	TIL-P	564	0	242	1.25	0.6	1340	1790
3	TIL FF 29%	400	164	242	0.75	0.6	1340	1790
4	TIL FF 37%	355	209	242	0.75	0.6	1340	1790
5	CG-P	564	0	242	1.00	0.6	1340	1790

WR - Water Reducer
FA- Class F Fly Ash
AEA - Air entraining agent

2.2. Mechanical Test Methods

Concrete mixing was carried out according to ASTM C192, with fresh tests such as slump (ASTM C143), air content (ASTM C231), and unit weight (ASTM C138). Setting times were inferred by observing temperature curves generated by the semi-adiabatic calorimetry. Table 4 shows the initial and final setting times of concrete mixtures obtained from the results of the semi-adiabatic device, taken at 20% and 50% of the highest temperature change [55].

Eighteen cylinders were cast for each batch of every concrete mixture. The compressive strength of concrete (ASTM C39) was tested in triplicate for statistical purposes at 7, 14 and 28 days. Admixture dosages were chosen by considering target slump as shown in Table 4. The w/cm ratio was kept constant at 0.43 to avoid discrepancy and for comparison purposes, also because it is the North Dakota Department of Transportation's (NDDOT) recommended ratio.

Admixtures can have a critical effect on the durability of concrete. Water reducers and air entrainment agents, depending on dosage, can be deleterious or beneficial for the durability of the concrete mixture. Therefore, to get a more in-depth look at the hydration process and the effect of admixtures, a semi-adiabatic calorimetry test was adopted. Two 4"x8" cylinders of each concrete

mixture were placed inside the semi-adiabatic calorimetry device and temperature development was measured for a minimum of 24 hours with a one-minute interval.

Free shrinkage test was carried out according to ASTM C157, the compressive test according to ASTM C39, the splitting tensile test according to ASTM C496 and the electrical resistivity test according to ASTM C1760 were also executed. On the electrical resistivity device, a high resistivity reading indicates low electrical conductivity due to the lack of pore fluid in the samples.

To measure restrained shrinkage, the ASTM C1581 standard ring test was carried out. The rings were put into a temperature-controlled room with optimal relative humidity. The data logging interval was set to ten minutes and readings were logged for at least 28 days.

Lastly, the freeze-thaw resistance of concrete was measured using the standard test method from ASTM C666. Three prisms for each of the five mixtures, 15+1* (1* - dummy prism) were cast, and the resonant frequency was measured according to ASTM C215. For measuring the resonant transverse frequency of the specimen, the impact resonance method was adopted.

2.3. Microstructure Study Test Methods

2.3.1. Paste Specimens

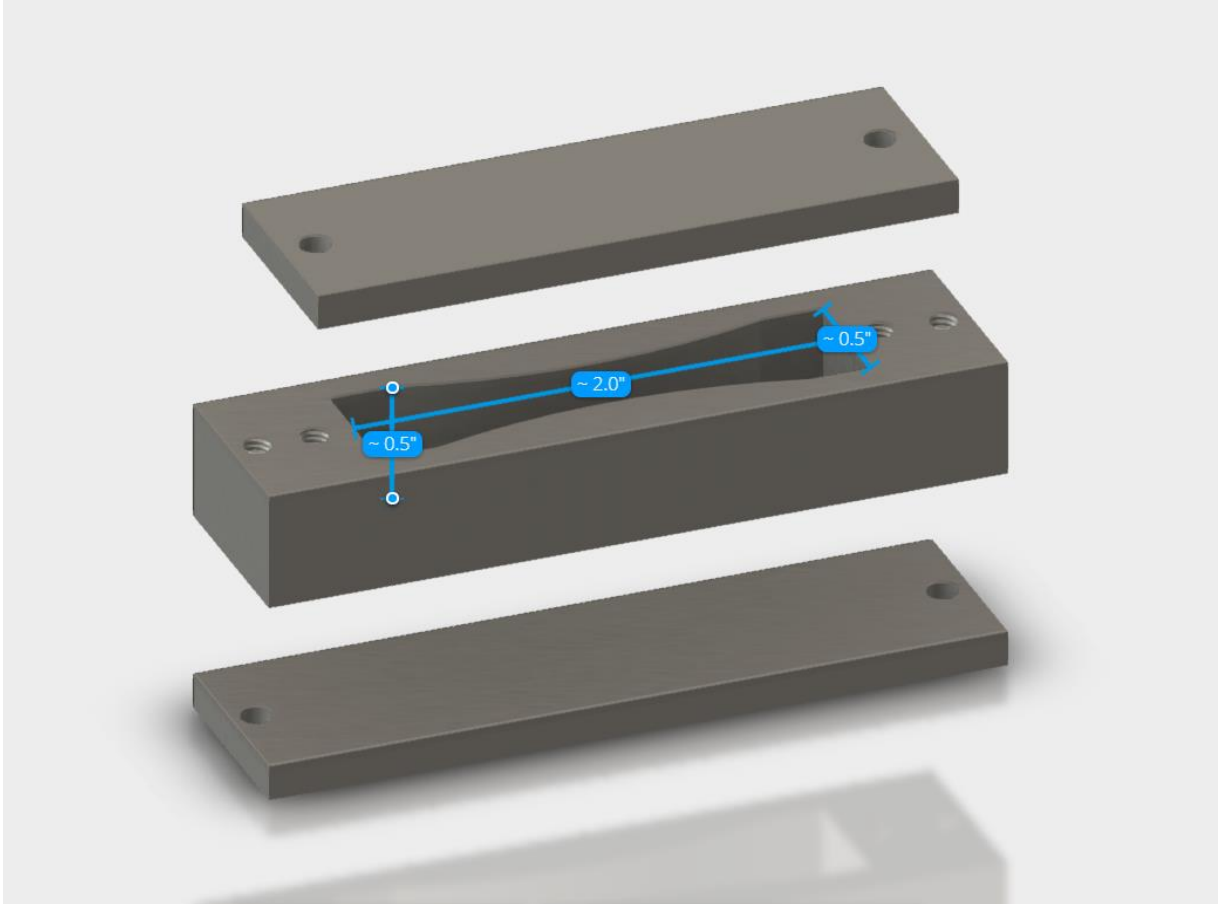

Figure 2: Paste specimen dimensions inside the 3D mold

Cement paste specimens were cast for all five cementitious mixtures selected for this study as described in section 2.1. Water to cement ratio was kept constant at 0.43 similar to the concrete samples. For microstructure studies, the mold was fabricated using a resin-based 3D printer called Form 2. A 3D CAD model was drafted using Autodesk Fusion 360. Additionally, the dimensions of the paste specimen and the overall 3D mold design rendered in A360 can also be observed in Figure 2. The mold was designed to cast the paste specimens in a particular hourglass shape to help induce cracks at the center. The dimensions of the specimen were 2”x0.5”x0.5” (Figure 2).

The hourglass shape was adopted to induce maximum drying shrinkage along the middle section of shape/specimens. The 3D mold consisted of two plates the bottom plate and the top plate which were fastened using pan-head machine screws (USS #4-40 x ½ in.), the threads were generated using the software and before printing. A total of 10 molds were printed, two for each mixture. The cement paste mixtures were prepared according to ASTM C305
[56]. These specimens were then attached to an end to end rotator (Figure 7) at 10 rotations per minute for 12 hours to promote even distribution of water and to minimize bleeding. Later the specimens were demolded (top and bottom mold plates were detached) (Figure 3) and allowed to dry according to ASTM C1581 [43] for 28 days.

Figure 3: Cured 3D mold paste specimens

2.3.2. Fluorescence Microscopy

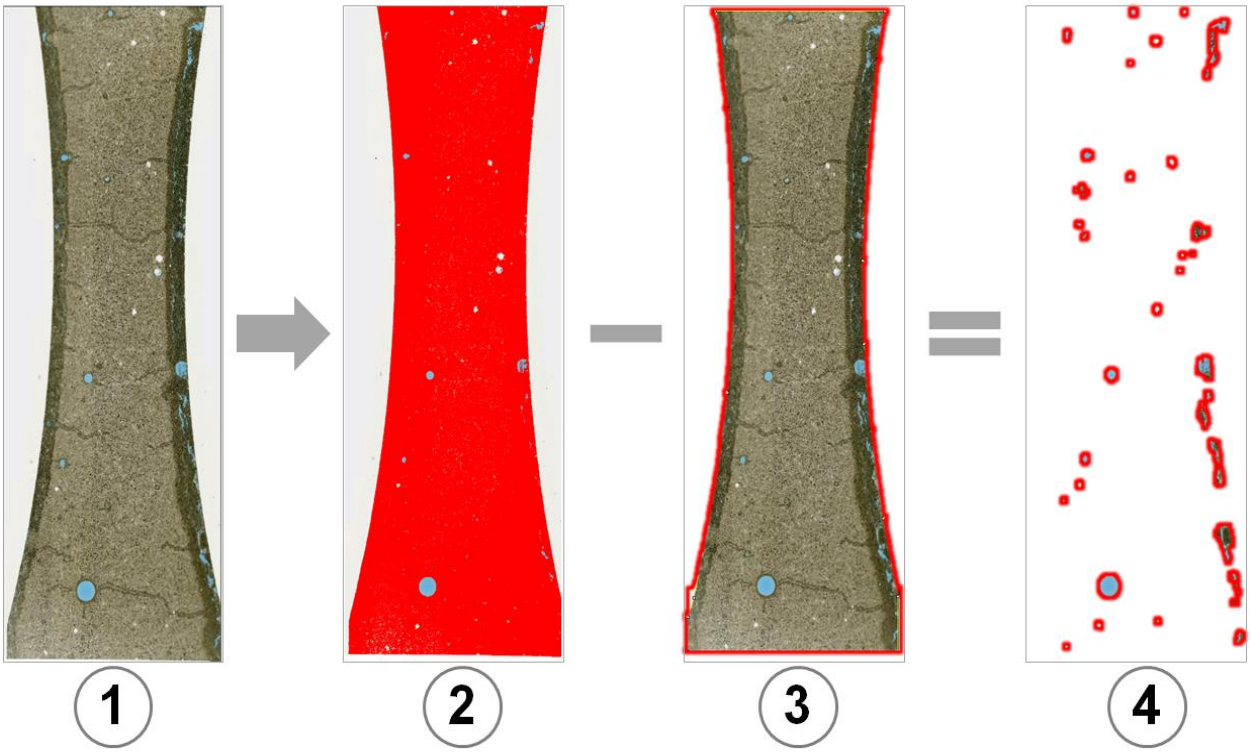

Figure 4: ImageJ2 analysis workflow

*1 - Original recorded image of the paste specimen
*2 - Only the paste, measure pixel^2 (Color Threshold Function)
*3 - Paste + Voids, measure pixel^2 (Selection Tools for the selecting outline and isolating bg.)
*4 - Only Voids/defect pixel^2 (Result)

During this process, the specimens were epoxy impregnated with a blue dye and petrographic slides of the specimen's sections (35μ) and cover slips were produced by an external professional laboratory. To make the thin slides a diamond saw was used. These thin slides were later observed under a confocal microscope at 40X magnification (Figure 5). Fluorescence was detected at an excitation wavelength of 488 nm. The recorded images were then analyzed by using an ImageJ2 software, using color threshold function. Which isolated the crack/defects area in terms of pixels^2 which is calculated as a percentage over total area of the specimen, as per Equation 1.

Figure 4 provides an overview of the workflow followed to obtain the void/defects % from the recorded images of the thin slides of each paste specimen.

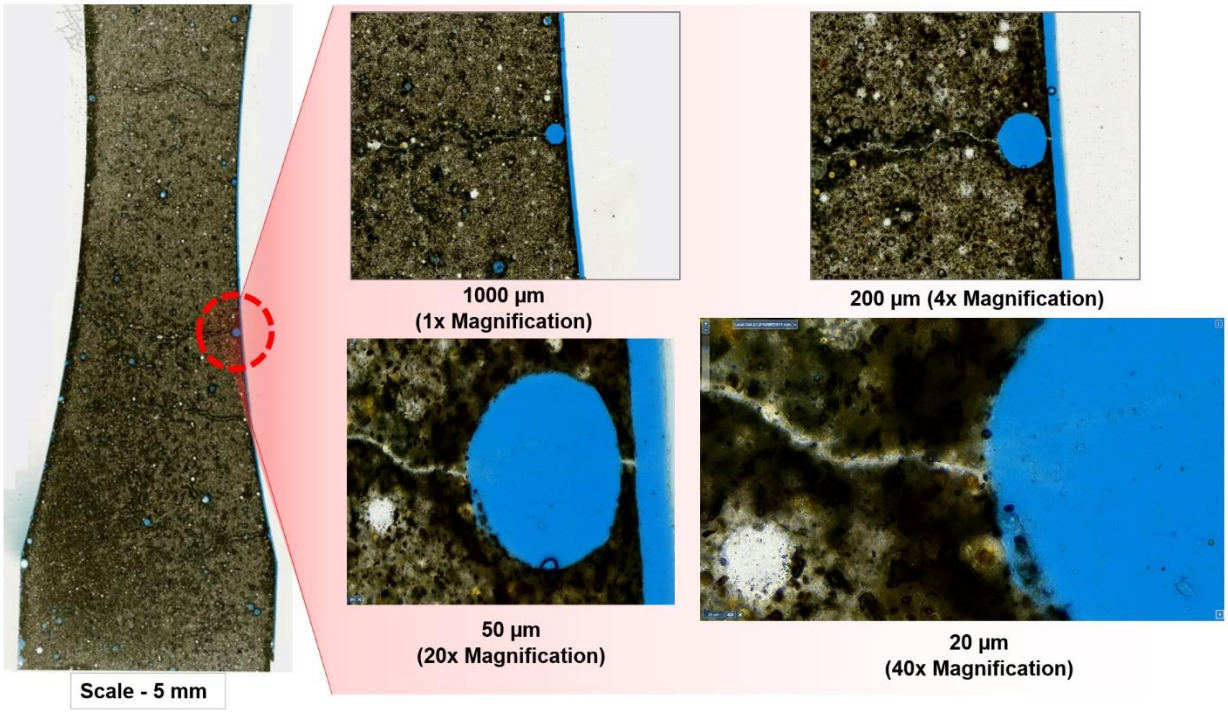

Figure 5: 40x magnification of slices of paste specimens, software PMA.start [85]

2.3.3. Micro-Computed Tomography (µ-CT)

Cured paste specimens inside their molds were exposed to X-ray µ-CT scan using a General Electric Phoenix V | tome | x s 240, located at NDSU Electron Microscopy Center Core facility. The specimens were scanned using a 180-kV x-ray tube running at 110 kV, 350A, exposure of 333 ms. A total of 1200 images (TIFF) were generated for each specimen. A commercial software package Volume Graphics Studio Max Version (VGStudio Max) 3.2 was used to reconstruct and analyze the volumes generated from the TIFF image files. Figure 6 shows the process of analyzing the specimen after µ-CT. For measuring the porosity, VGEasyPore pore analysis function was selected in VGStudio Max. Initially, the surface determination mode was used to isolate the paste specimen from the 3D mold material using a histogram. A threshold value

was specified to help fine tune the selection process and was further optimized using iterative surface determination mode. This method was followed the same for the rest of the specimen. Although in theory, the surface determination histogram could be manually fit to detect and quantify defects/voids as small as 30µ, for a linear comparison of the porosity of void size 75 µ and higher, among the chosen cement paste combinations the default method has been considered adequate [57]. After a surface determination is completed, VGEasyPore Analysis function was used with a minimum voxel size set to 8 voxels, and the minimum probability of voids set to 2. Figure 6 shows a 3D mesh exported after the analysis to showcase the data gathered through the procedure.

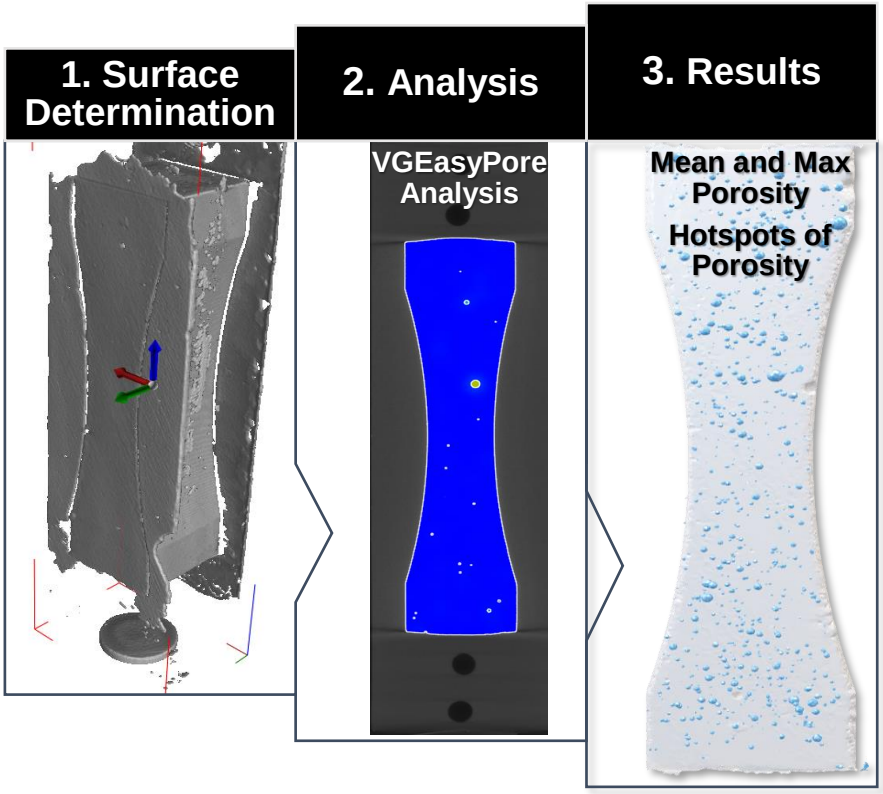

Figure 6: Workflow to analyze µ-CT data for the paste specimen

Figure 7: End to end rotator

3. RESULTS AND DISCUSSION

3.1. Mechanical Test Results

3.1.1. Fresh Properties

3.1.1.1. Workability

Table 4: Fresh properties

Mix Code	Fresh properties				
	Slump (in)	Air (%)	Unit weight (lb./ft^3)	Setting Time from calorimetry (minutes)	
				Initial (20% Temperature Rise)	Final (50% Temperature Rise)
T I/II FF 29%	4.25	7.6	142.27	136	343
TIL-P	4.00	7.2	141.74	272	409
TIL FF 29%	6.00	7.4	139.27	272	442
TIL FF 37%	6.00	6.8	141.21	244	405
CG-P	5.00	8.0	139.80	315	467

The slump was set to around a typical 4 - 6 inches range. Workability of the concrete mixture is critical for its adoption, hence maintaining a good slump was considered crucial. From Table 4, the mixtures without fly ash required a higher dosage of water reducer to achieve the targeted slump value and vice versa. Overall, the inclusion of fly ash usually resulted in increased workability; this could be attributed to fly ash particles which are known to have a spherical shape that could lead to a lubricating effect to the mixture [58]. This effect was prominent in the Type IL cement mixtures.

TIL-P mixture was observed to have the lowest slump of all mixtures, which could be due to the substitution of portland cement with limestone (10%), as well as the absence of fly ash. The CG-P mixture gave adequate slump with a moderate dosage of water reducer, which could be due to coarser cement particles.

3.1.1.2. Air Content (%)

Table 4 shows the air content % for the chosen mixtures. The air content (%) was maintained at the typical local range of around 5 - 8% [35]. Tests like freeze-thaw resistance require an adequate amount of entrained air content combined with a proper air-void system [6].

3.1.1.3. Setting Time

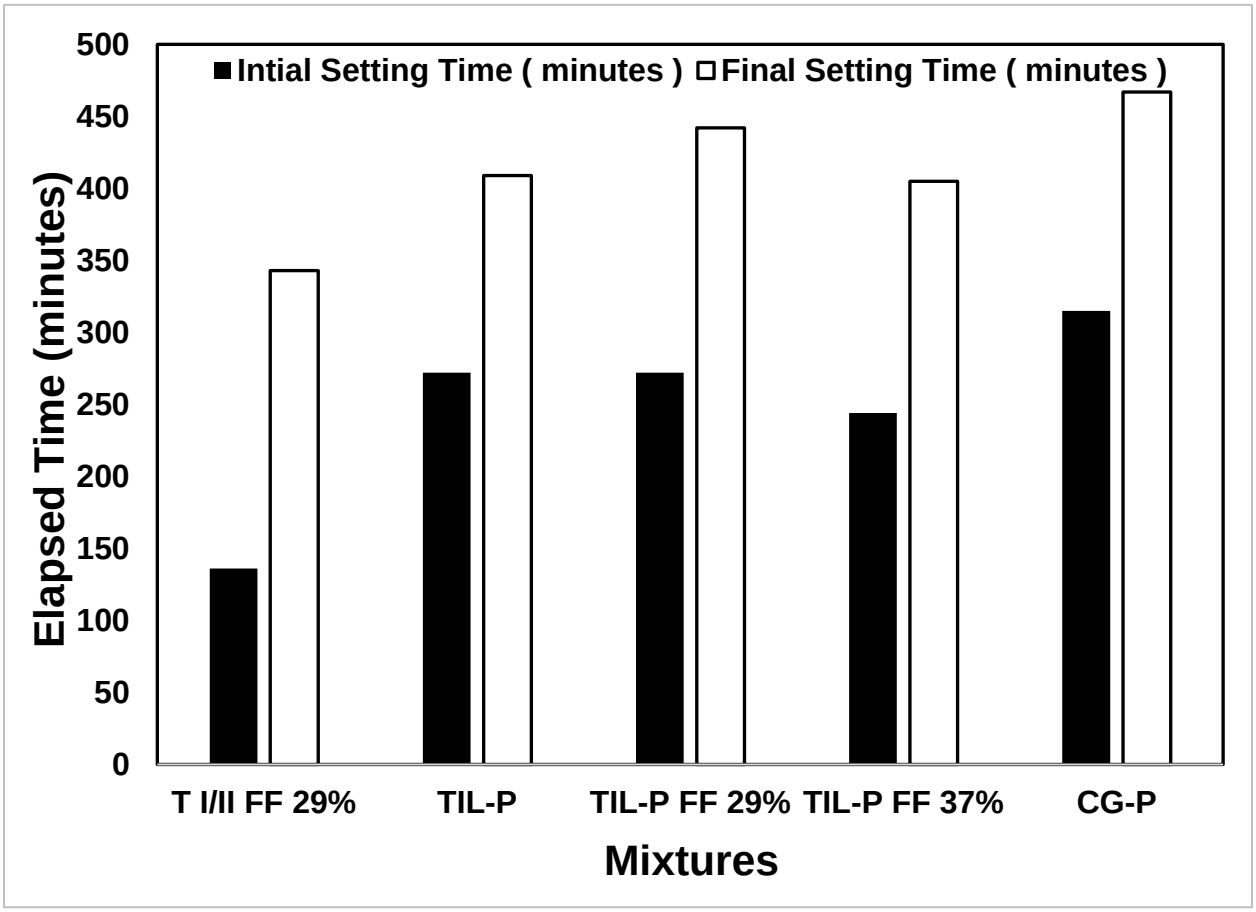

Figure 8: Setting time of concrete mixtures

Figure 8 shows the Initial and final setting times which were calculated from 20% and 50% of peak temperature change observed in semi-adiabatic calorimetry results (Figure 9) [55]. Mixtures without fly ash were seen to have lower setting times compared to mixtures with fly ash. Incorporation of fly ash, especially in higher volumes, is known to impede the hydration process

[59]. In contrast, the results show that in Type IL cement-based mixtures with high fly ash (%) the setting times were similar to TIL-P cement mixture. This reduction in setting time could be due to the nucleation effect provided by the limestone particles [60–62]. Thus the addition of limestone could help reduce the dilution effect of fly ash, resulting in a reduction of setting times [63]. Also, it is claimed that the addition of limestone accelerates tri-calcium silicate (C_3S) hydration and forms calcium carboaluminate hydrates while reducing the formation of the more unstable ettringite [64].

However, in comparison to the TI/II mixture, Type IL cement-based mixtures had longer setting times. Interestingly, they were still lower in comparison to the CG-P mixture [65].

3.1.1.4. Semi-Adiabatic Calorimetry

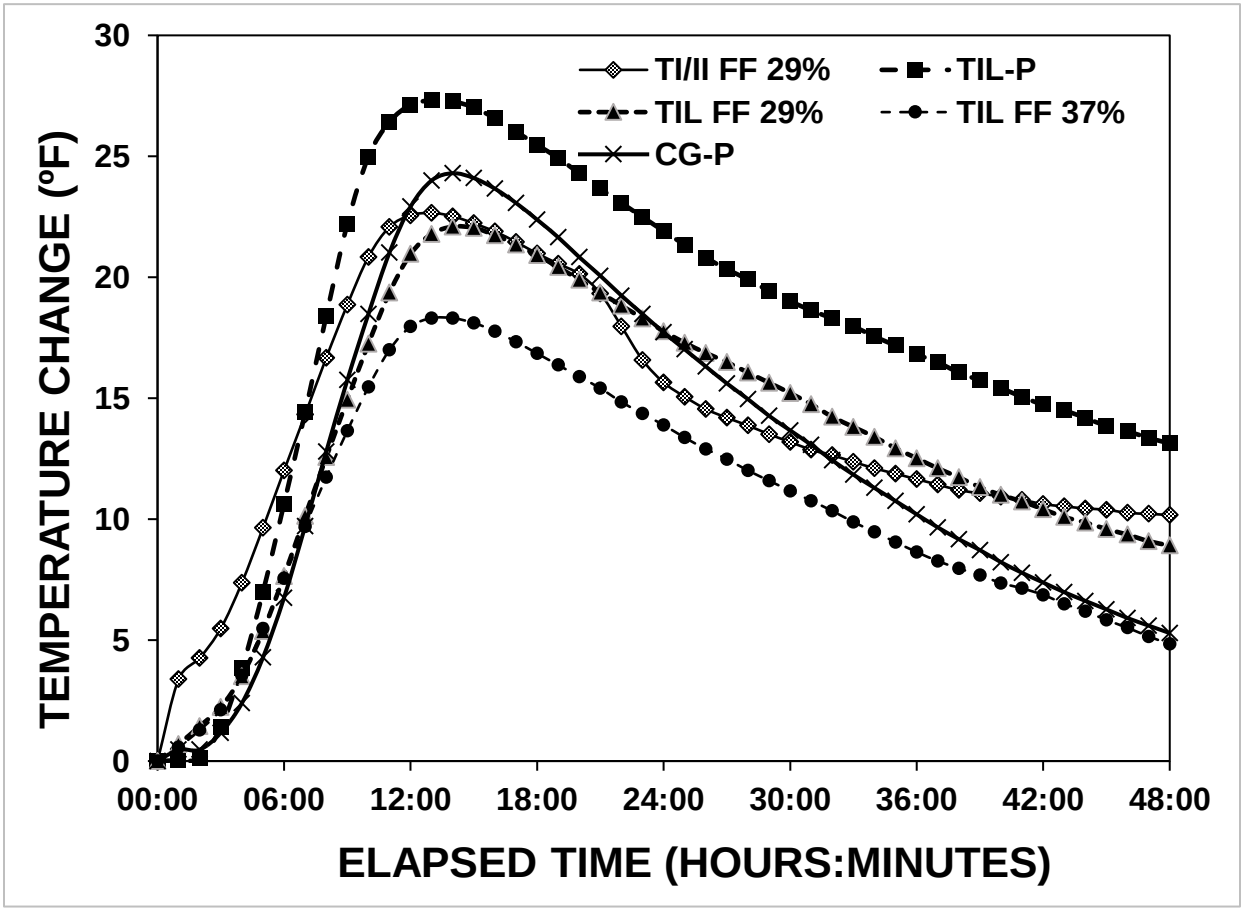

Figure 9: Degree of hydration as measured through semi-adiabatic calorimetry

Figure 9 shows semi-adiabatic calorimetry results and Figure 10 shows the instrument used for the test. TIL-P showed the highest temperature change of all the mixtures. This is consistent with the previous literature, showing that limestone particles promote heterogeneous nucleation of hydrates, leading to an acceleration of the hydration process [60,61,66].

The second highest temperature change is seen in CG-P, but the initial rate of hydration is delayed as compared to other mixtures. The coarser cement particles lead to a slower hydration process that, in turn, could be beneficial to prevent cracking due to thermal gradients [26,65].

Even though TIL FF 29% and TIL FF 37% both exhibit similar initial hydration processes, the effect of additional fly ash is clearly visible when their peak temperature changes are observed. The hydration acceleration period is shorter in case of TIL-FF 37% in comparison to TIL-FF 29%.

Interestingly, the TI/II-FF 29% curve exhibited sulfate depletion. This could be attributed to consumption of sulfate due to the abundance of portland cement content (in comparison to PLC mixtures) and fly ash (29%).

Figure 10: Semi-Adiabatic calorimetry instrument (F Cal 4000)

3.1.2. Hardened Properties

3.1.2.1. Compressive Strength and Splitting Tensile Strength

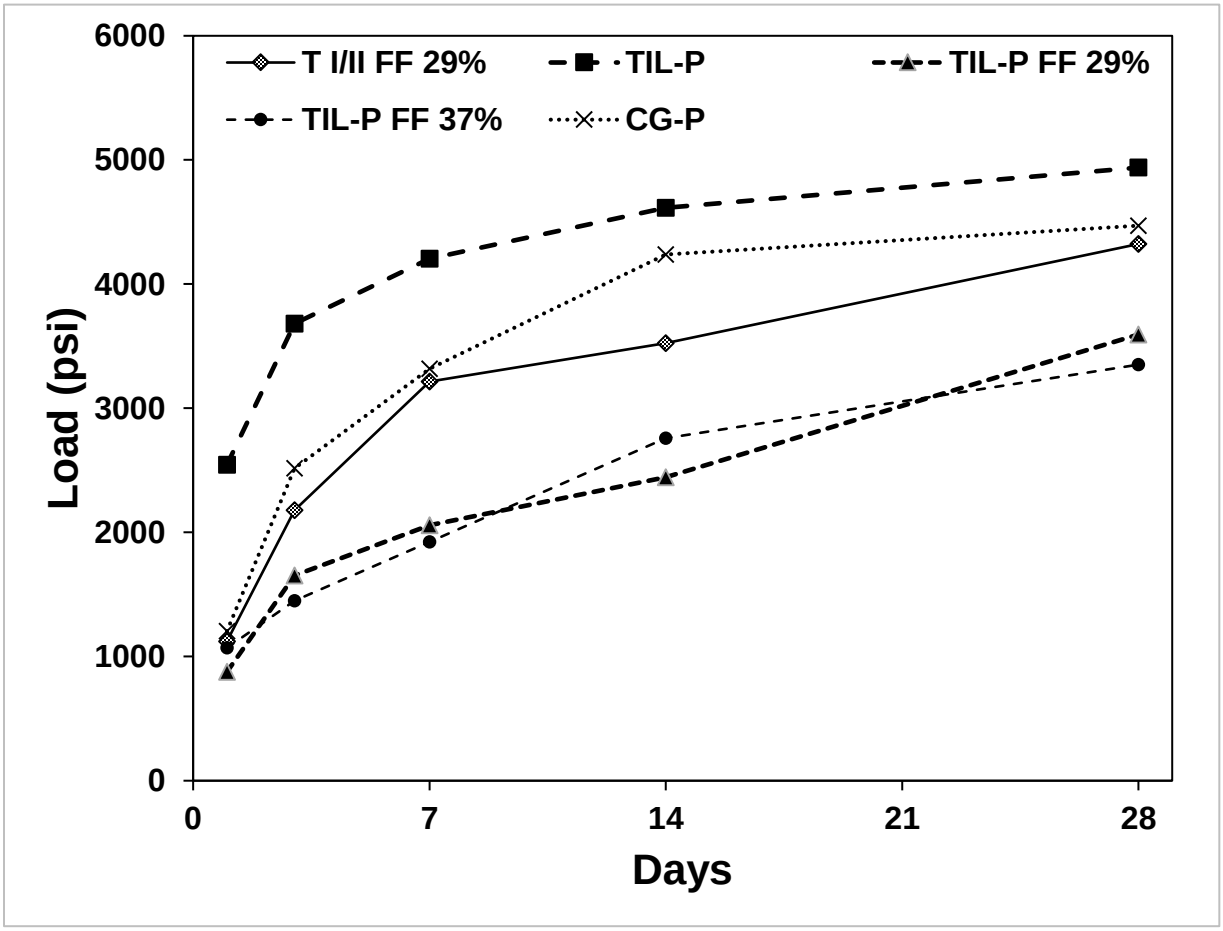

Figure 11: Compressive strength

The compressive strength of the concrete mixtures is shown in Figure 12 shows concrete specimens after failure from strength tests. Figure 11 shows the results for compressive strength test. The highest compressive strength was measured for the TIL-P mixture. This is in line with previous studies and could be explained by better particle size distribution [19], the formation of more stable hydration products like carboaluminates [17,61,64] and accelerated cement hydration due to the nucleation effect of limestone particles [60,61], leads to higher early compressive strength. The lowest compressive strength was measured for TIL-FF 37% and the

second lowest was measured for TIL-FF 29%. Incidentally, the TI/II FF 29% mixture performed relatively better than the TIL FF 29%. It is known that incorporation of fly ash improves long-term strength gain and increased cementitious material in the mixture helps with early strength gain [67]. The strength gain in the Type IL cement-based fly ash mixtures follows this trend; due to lower cementitious content in the mixture and high fly ash content, the early strength is lower. However, because of additional C-S-H gel formation [25], fly ash could help increase compressive strength beyond the 28 day period [68]. Figure 13 shows the results of the 28-day splitting tensile strength test. Except for the CG-P, the results were similar to the compressive strength results. Splitting tensile strength was observed to decrease with increase in fly ash content. Similar to the strength test, previous studies indicate that high volume fly ash-based mixtures have slow development of strength [69] while the addition of fly ash to concrete has a very subtle effect on splitting-tensile strength results [70].

Figure 12: Failure of specimens during strength

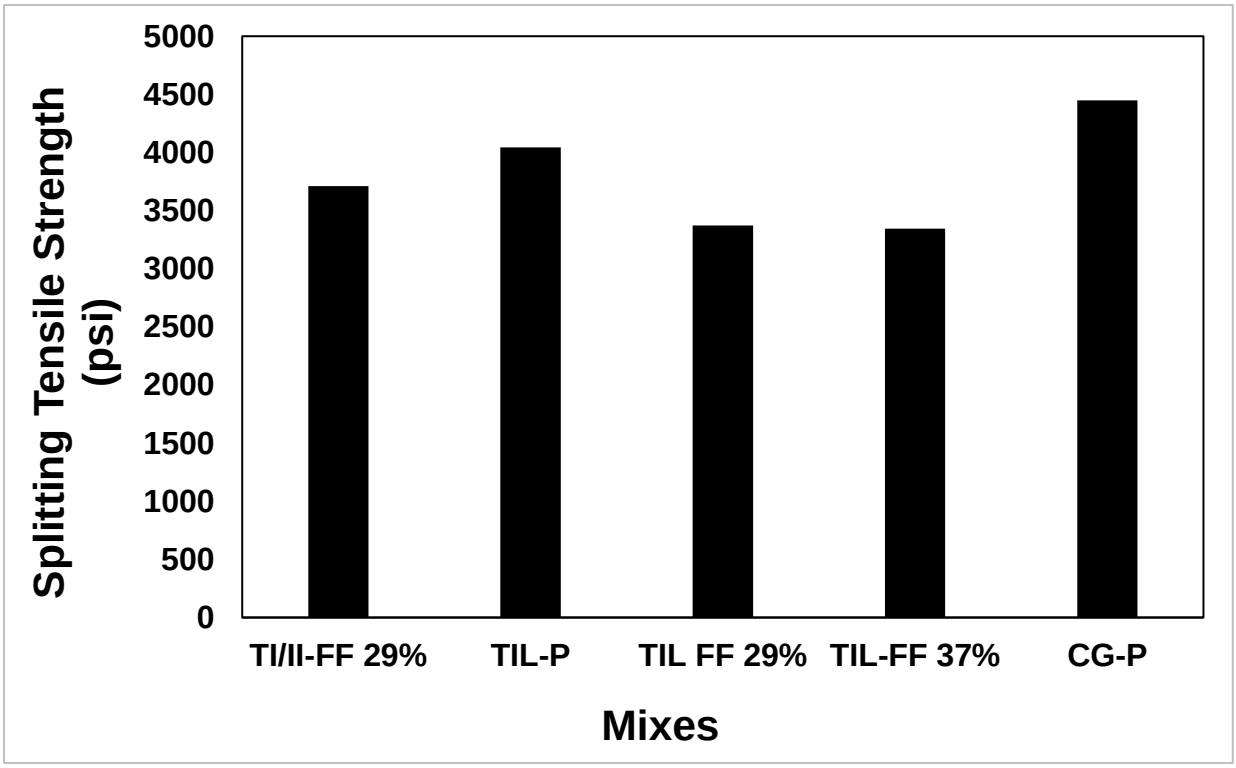

Figure 13: Splitting tensile strength

3.1.2.2. Resistivity

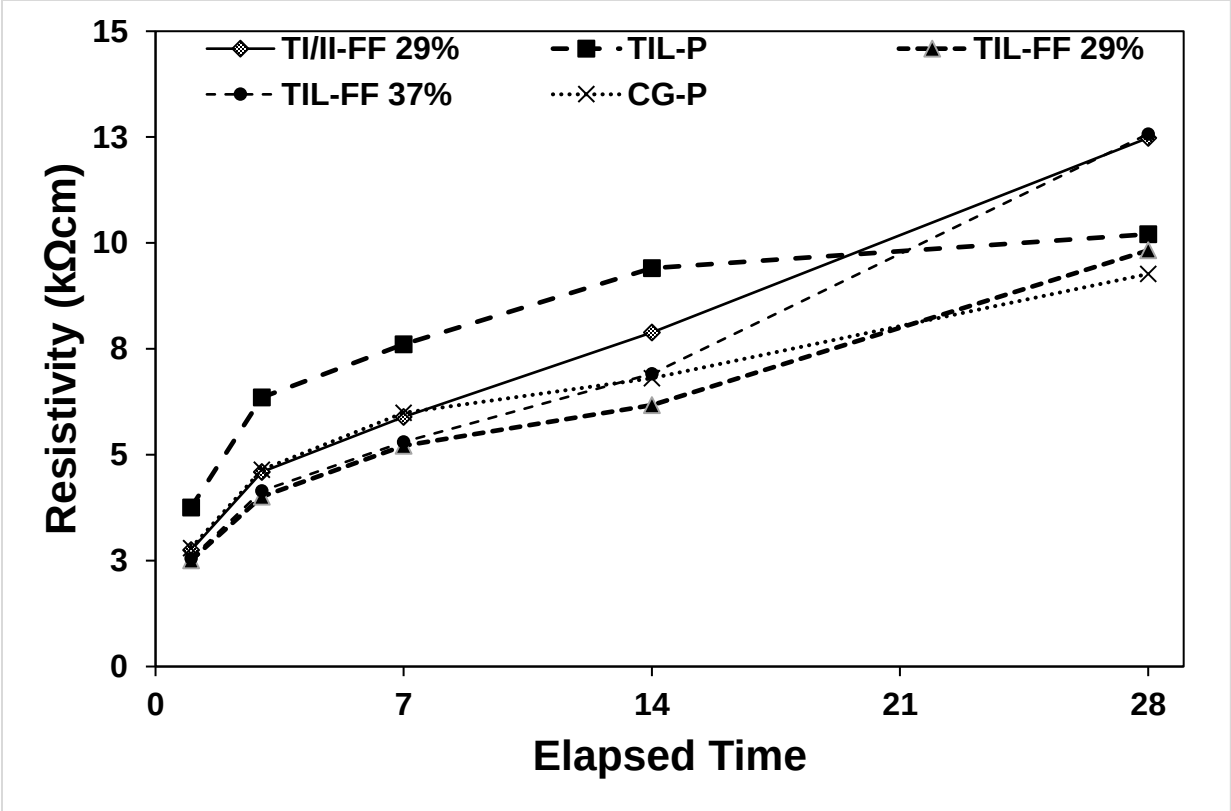

Figure 14: Electrical resistivity

Resistivity test results are presented in Figure 14 measured using the Resipod instrument (Figure 15). Resistivity is used as a value to measure the resistance of concrete to the ingress of deleterious ions like Chloride ions. In other words, it can be used as an indirect measure of the permeability of the concrete mixture [6]. Permeability can be related to pore structure and microstructure [71]. One of the many benefits of measuring the electrical resistivity test is that it can be taken at any point during the lifecycle of the specimen under any environmental conditions [72].

The highest resistivity was measured for both the mixtures TIL-FF 37% and TI/II-FF 29%. The fly ash-based mixtures showed better results in comparison to plain cement-based mixtures, especially after fourteen days and beyond. Fly ash is known to improve the microstructure of concrete due to extended pozzolanic reactions over more extended periods of time [25,73]. In addition, the nucleation effect of the fine limestone particles also aid in the refinement of the pore structure of Type IL cement mixtures [71].

Course ground cement mixture is known to have porous microstructure due to larger cement particles, and therefore the resistivity results are comparably lower [74].

Figure 15: Electrical resistivity test equipment (Resipod Proceq)

3.1.2.3. Free Shrinkage

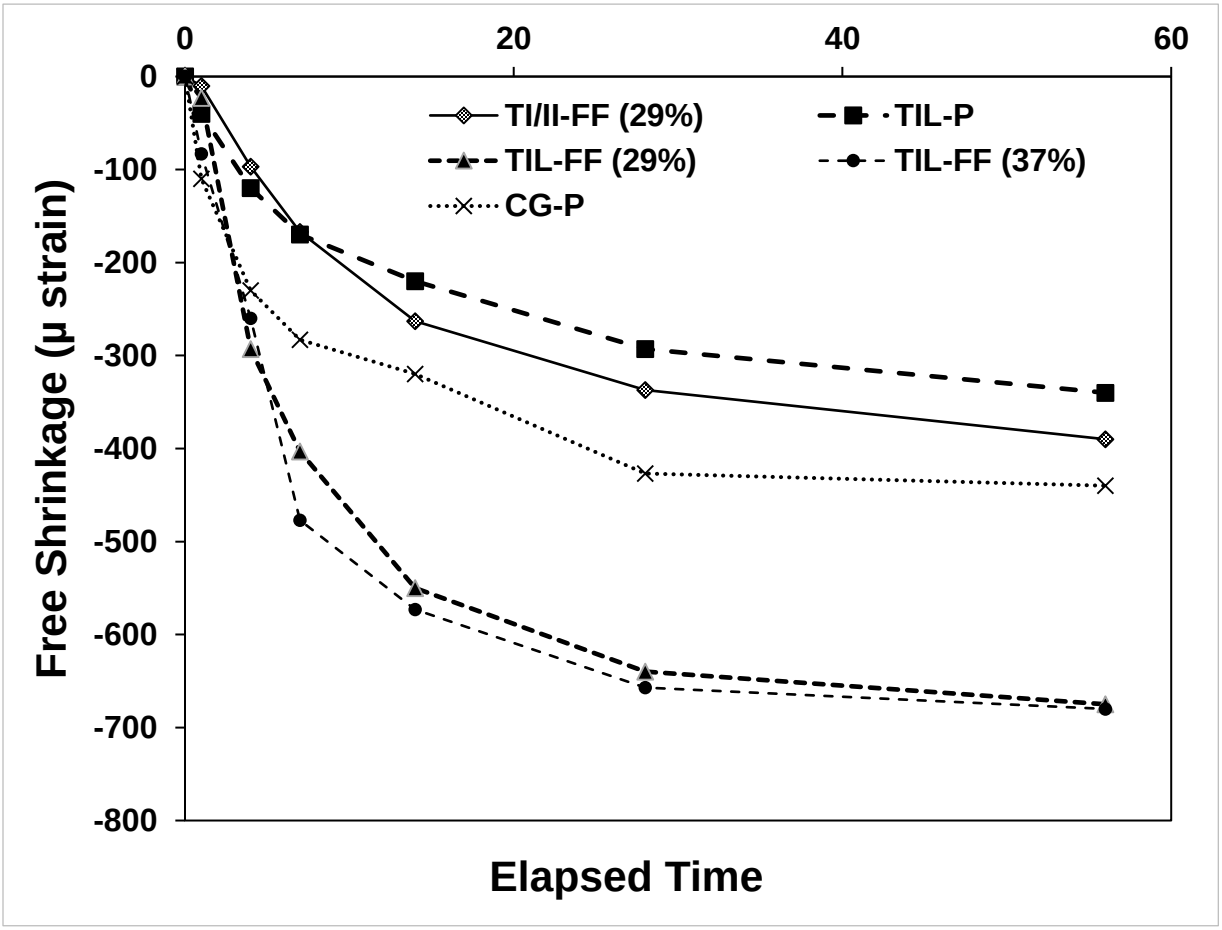

Figure 16: Free shrinkage

The results for free shrinkage strain of the mixtures can be seen in Figure 16, the length comparator device used for this test is shown in Figure 17. As stated in section 1.3, with the Young-Laplace relationship it can be inferred that finer cement like PLC could lead to more shrinkage due to a higher amount of smaller pore formation. However, prior researchers [75] suggested that the idea of capillary stress may not be alone responsible, and there could be other dynamics involved in the shrinkage development, especially at pore size lower than 100µm.

Finer cements are known to develop smaller pores, suggesting higher levels of capillary stress development and thereby increased shrinkage. Meanwhile, during manufacturing of PLC

the intergrinding of limestone results in a reduction of larger cement particles and limestone particles occupying the smaller size ranges [76]. Hence, the PSD in PLC shows an increase in smaller pores (1-2 nm, also known as gel pores) where the idea of capillary stress due to the formation of the meniscus may no longer be as valid, and other mechanisms control shrinkage development [12,75]. Hence, this could explain low shrinkage results in the TIL-P based mixture.

TIL-P exhibited the lowest free shrinkage strain. Going by the trend of the curves, it should be noted that the CG-P shrinkage strain could be considered lower overall. Addition of fly ash is known to increase drying shrinkage strain [77] in the mixture.

TIL-FF 29% and TIL-FF 37% both exhibited higher free shrinkage strain. This could be explained due to the higher availability of free water in the concrete mixtures containing fly ash, as concrete with fly ash requires less water to achieve similar consistency than concrete without fly ash [78,79].

Figure 17: Free-shrinkage testing instrument

3.1.2.4. Restrained Shrinkage

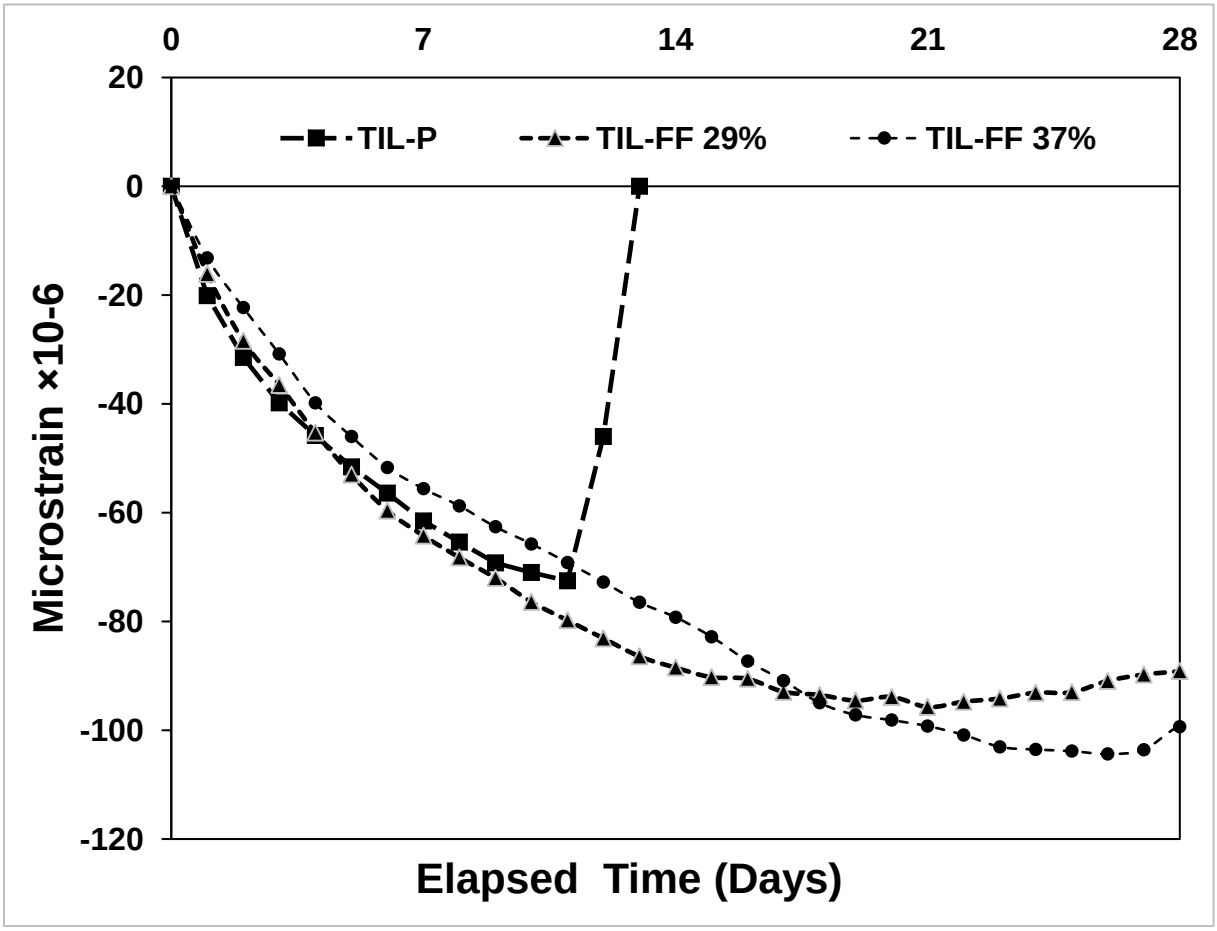

Figure 18: Restrained shrinkage

For the restrained shrinkage test (Figure 18), three promising mixtures were chosen based on the other tests conducted. For TIL-P mixture results, it can be observed that the ring (Figure 19) was cracked around twelve days elapsed time, while the other two rings, TIL-FF 29% and TIL-FF 37%, did not crack.

Prior researchers [27] have also reported early age cracking for the PLC-based mixture in ring tests. It was reported that PLC experiences a slightly higher expansion in comparison to other materials (FA, cement particles) immediately after setting, and this may lead to earlier cracking because the resulting shrinkage due to expansion caused by limestone would be higher in PLC.

After examining the results, it can be inferred that the addition of a high volume of fly ash in portland limestone concrete mixtures could make them more resistant to cracking under restrained shrinkage condition. This could be explained by the addition of both fly ash and limestone in the mixture. Not only does the fly ash enhance the mixture by adding a filler effect but also by the secondary formation of C-S-H. Fly ash used in the mixture (Class F) is known to add more aluminate during hydration. The additionally available aluminates in the mixture combine with the limestone to facilitate the formation of more carboaluminates [61].

Figure 19: Ring testing arrangement.

3.1.2.5. Freeze-Thaw Test

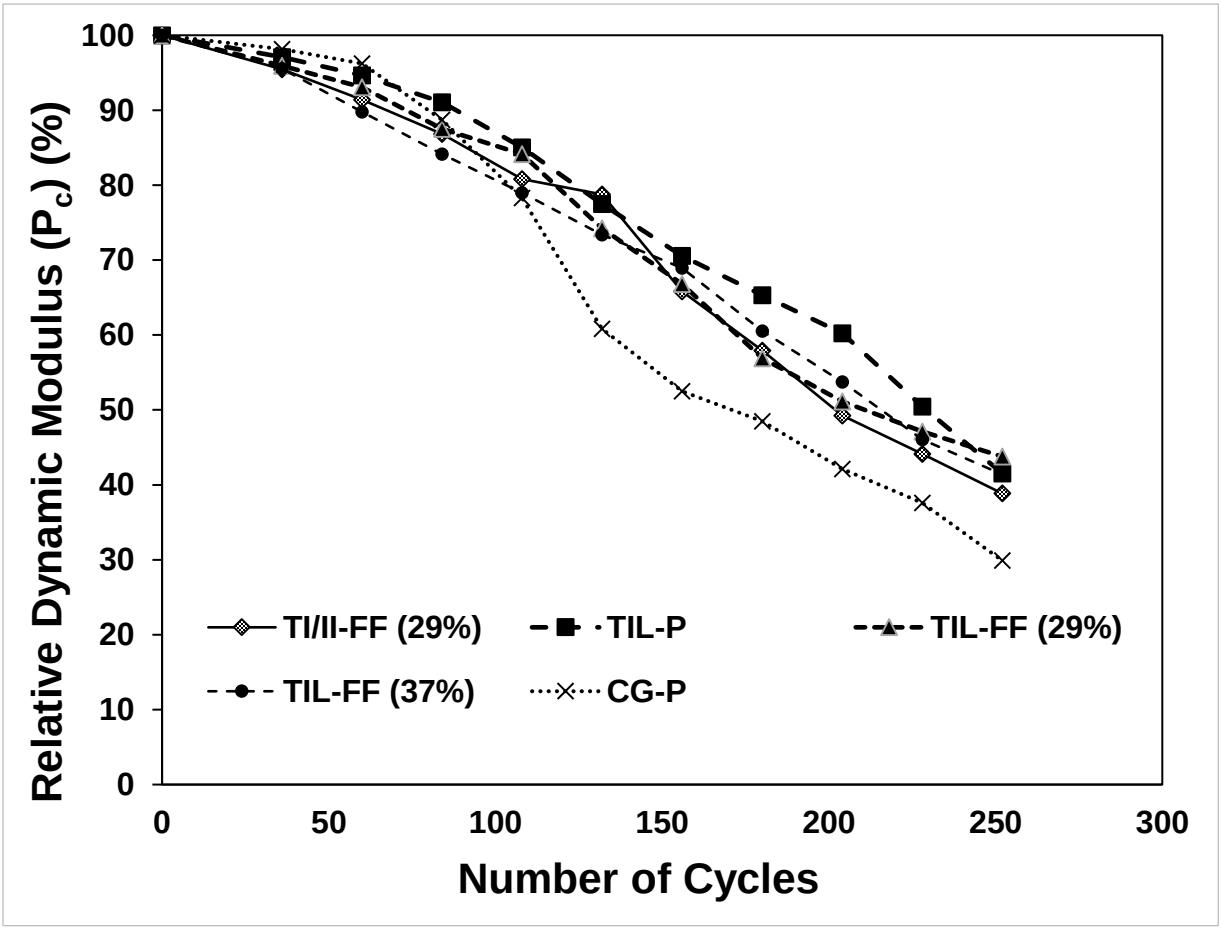

Figure 20: Freeze-Thaw test results

Table 5: Durability factor at 60% P_c

Mixtures	**Cycles at 60% P_c**	**D.F at 60% P_c**
T/II FF 29%	180	35.96
TIL-P	204	40.86
TIL-FF 29%	180	35.96
TIL-FF 37%	180	36.00
CG-P	132	26.45

Figure 20 shows a graph containing relative dynamic modulus plotted against a corresponding number of freeze-thaw cycles. TIL-P showed the highest freeze-thaw resistance, and mixtures containing fly ash showed results similar to each other. At 300 cycles, all five

mixtures had a relative dynamic modulus of elasticity (%) of < 60%, which is recommended by ASTM C666. Figure 21 shows the concrete specimen inside the freeze-thaw chamber, and Figure 22 shows the Impact resonance test equipment used to measure resonant frequency to further find the relative dynamic modulus of the specimens as per ASTM C666.

The freeze-thaw resistance of the concrete mixture is based heavily on the amount of air content (%). Adding an air-entraining agent introduces 0.05 to 1-mm of air bubbles, also known as entrained air voids, into the concrete mixture. The formation of these air voids helps elevate the hydraulic pressure formed by the capillary water during freezing and thawing cycles by acting as pressure relief and as escape boundaries [4].

Table 5 shows the durability factor at 60% P_c of all the concrete mixtures. The TIL-P mixture showed the maximum resistance in this test, failing after 204 cycles. Studies indicate that the concrete containing portland limestone cement have improved microstructure due to better particle size distribution and physical filling of interfacial transition zone by carboaluminate hydrates [80].

According to Mehta and Monteiro, “In general, the higher the water-cement ratio for a given degree of hydration or vice versa, the higher will be the volume of large pores in the hydrated cement paste,” [4]. In reference to that, the fly ash-based mixtures had higher water-cement ratios in comparison to plain cement mixtures. This could explain their comparatively lower results. The semi-adiabatic calorimetry also shows a similar trend in the hydration heat curves.

Some previous studies on Type-IL concrete with limestone (10%), have been observed to fail at 141 cycles [81]. Comparably, the data from this study shows that all portland limestone cement mixtures with fly ash were able to achieve more than 141 cycles and exhibited better freeze-thaw resistance compared to the control mixture (i.e., TI/II FF 29%, whose relative dynamic

modulus reached 60% at 132 cycles). All the mixtures showed increased scaling after 100 cycles of freezing and thawing.

Even though the CG-P showed better resistance in earlier cycles, it decreased rapidly after 100 cycles. Courser cement concrete mixtures are known to have larger pores in the microstructure [74], thus making them more vulnerable to the volume change of pore water during freezing and thawing.

Figure 21: Freeze-Thaw test prisms

Figure 22: Impact resonance test equipment

3.2. Microstructure Study Results

3.2.1. Fluorescence Microscopy

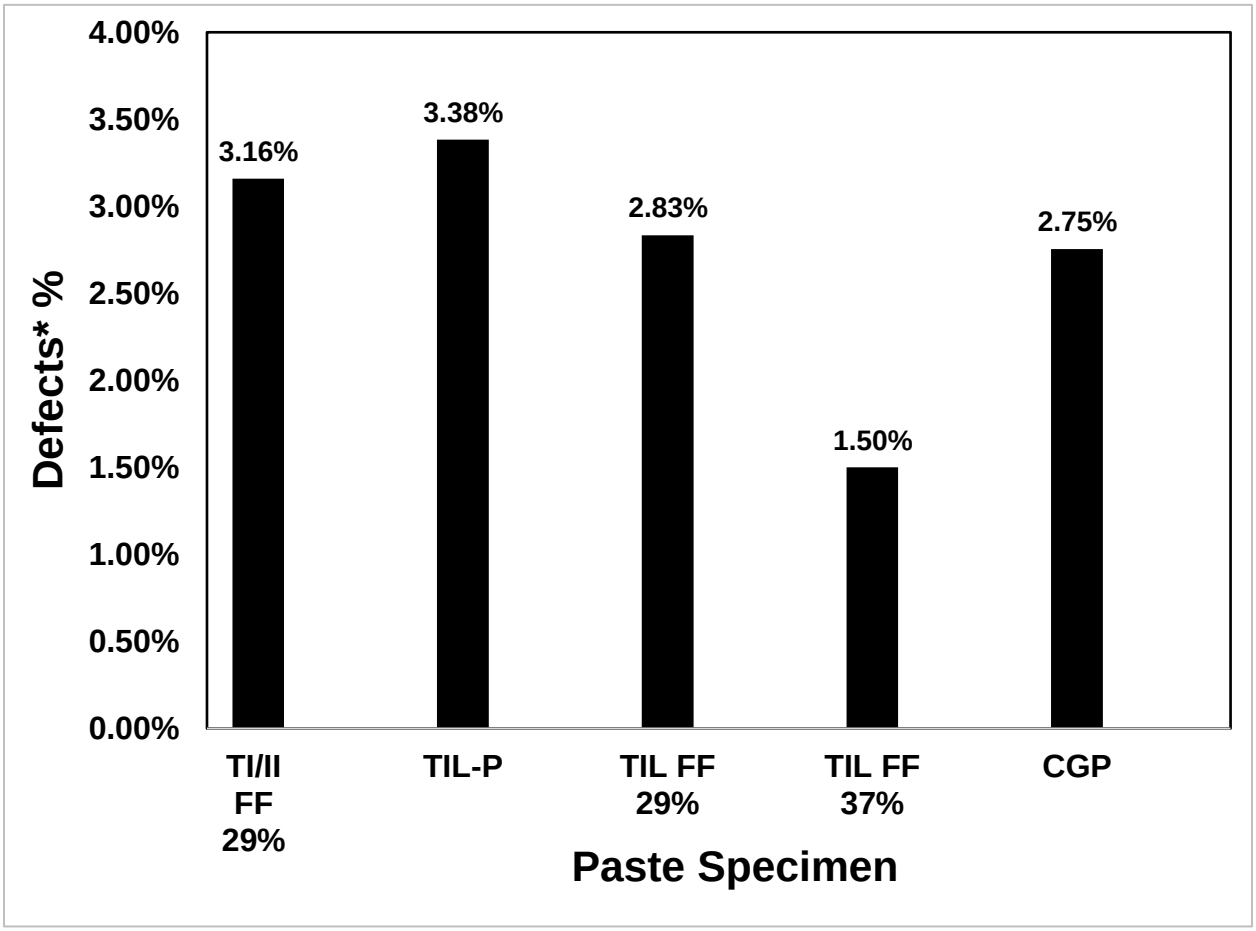

Figure 23: Average defects % of FM 3D mold specimen using ImageJ analysis

* Defects % = Voids + micro-cracks

From Figure 23, it may be observed that the lowest defects %, which is measured in terms of micro-pores and micro-cracks pixel^2 areas, is exhibited by TIL-FF 37%. This is, however, not reflected in case of the frequency of defects as observed through µ-CT. This may indicate a large number of voids left by free water due to fly ash in the paste with unaltered water-cementitious materials ratio (i.e., lower quantities of water are required to maintain similar workability). However, these voids are likely discrete and discontinuous in nature.

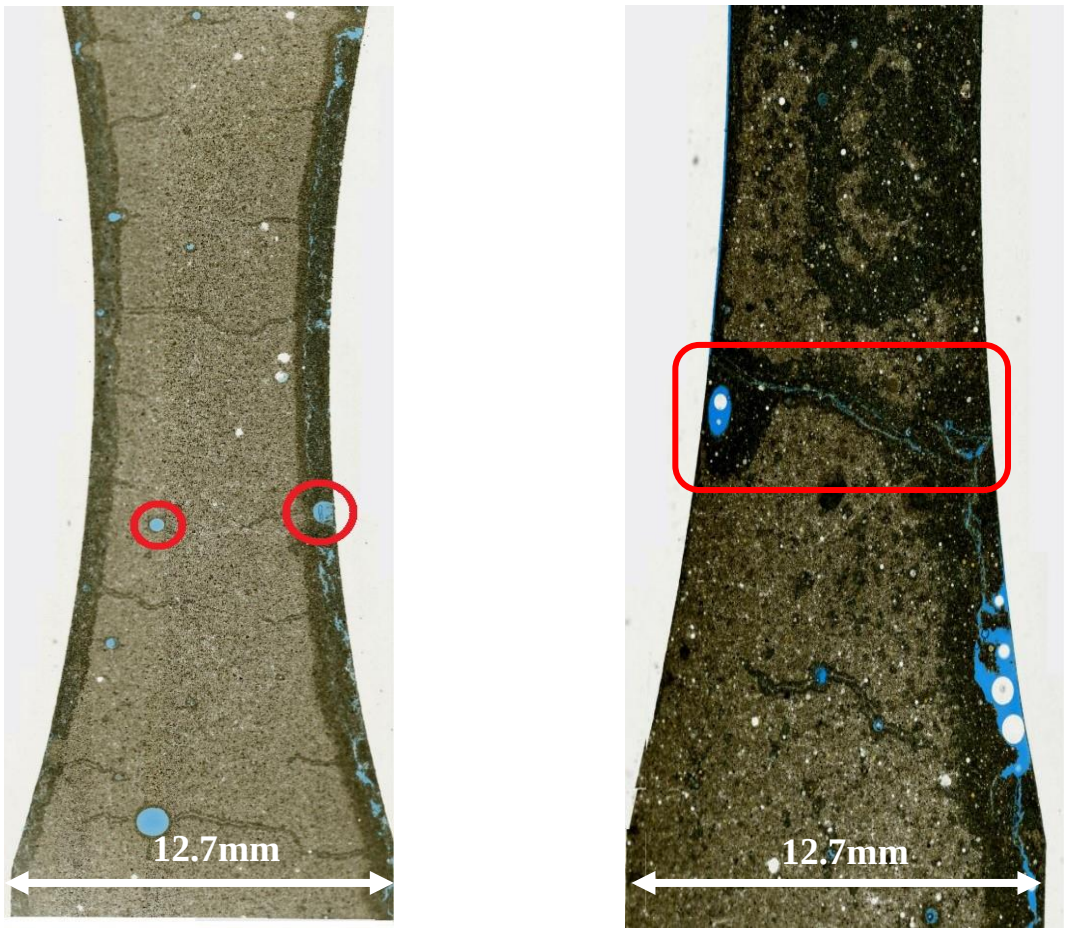

Figure 24: FM paste slices for TIL FF 37% (left) and CGP (right)

As a result, micro-cracks are not observable. The presence of many discontinuous voids is also evident in the case of Figure 24. The crack area visible in the central region of the sample, due to the geometric shape of the mold used. It was designed this way so that potential micro-cracks are created in the central region for ease of detection and visualization. Contrastingly, a smaller number of larger voids may be seen in case of CG-P (Figure 24). Cracks appear to originate between such voids, thus revealing continuity. The crack area as per Figure 24 is also higher in case of CG-P. This also explains the lower electrical resistivity of CG-P compared to TIL-FF 37%. A similar argument may also be put forward for TIL-P.

3.2.2. µ-CT Results

3.2.2.1. Void Size Distribution (µ-CT) vs. Electrical Resistivity

Electrical resistivity is an indirect indicator of the ability of concrete to prevent the ingress and subsequent flow of deleterious chemical ions such as chloride and sulfate. The long-term durability of concrete depends upon this ability of concrete. It is known that concrete is a poorer conductor of electricity than water (pore water in this case). It is evident that a concrete system with interconnected pores filled with pore fluid will be more conductive compared to one without a well-connected network of pores [82].

Another aspect of electrical resistivity in concrete will be the nature of pores, frequency or occurrence in a 3D space, and the degree of interconnectivity [40,42]. The mean porosity of a paste sample may not necessarily speak about its permeability. A closer look at the distribution of pores/voids inside a paste sample can reveal the nature of interconnections, if any, within the sample. The occurrence of a higher number of smaller voids/defects in a sample may be preferable than that of a lower number of larger defects. A discontinuous system of smaller defects filled with more conductive pore fluid inside a paste sample will result in higher electrical resistivity [82]. Contrastingly, from the perspective of conductivity, a more continuous system of larger defects filled with pore fluid may facilitate the passing of electrons and other deleterious chemical ions. This is manifested in case of some of the cementitious combinations in this study. Figure 25 reveals a higher frequency of defects (of all sizes), i.e., the number of defects detected in TI/II-FF 29% compared to CG-P under similar conditions of analysis. From the frequency histograms shown in Figures 26, it is evident that the paste sample of TI/II-FF 29% contained significantly higher number of smaller defects (between 300 and 500 µm in diameter) than larger ones (>500 µm) compared to a nearly uniform distribution of smaller and larger defects in case of CG-P.

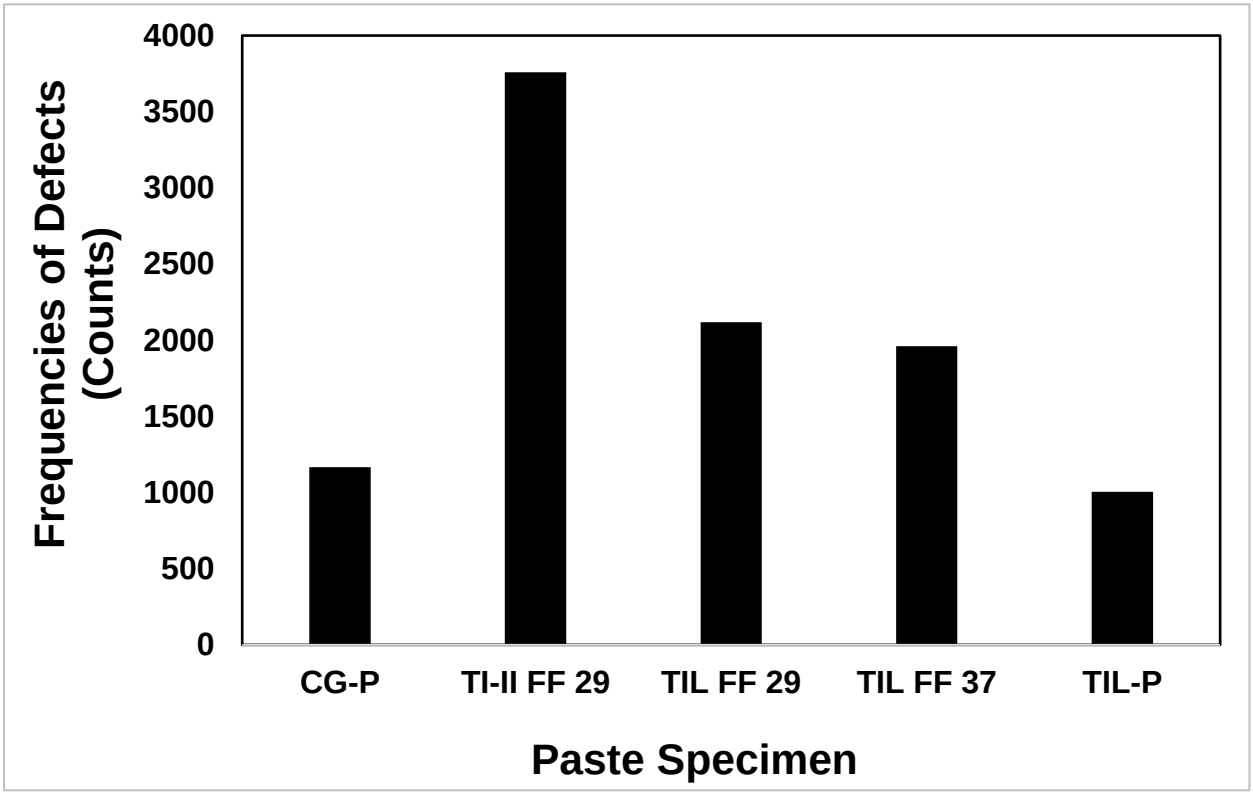

Figure 25: Frequencies of defects comparison of different paste specimen of µ-CT

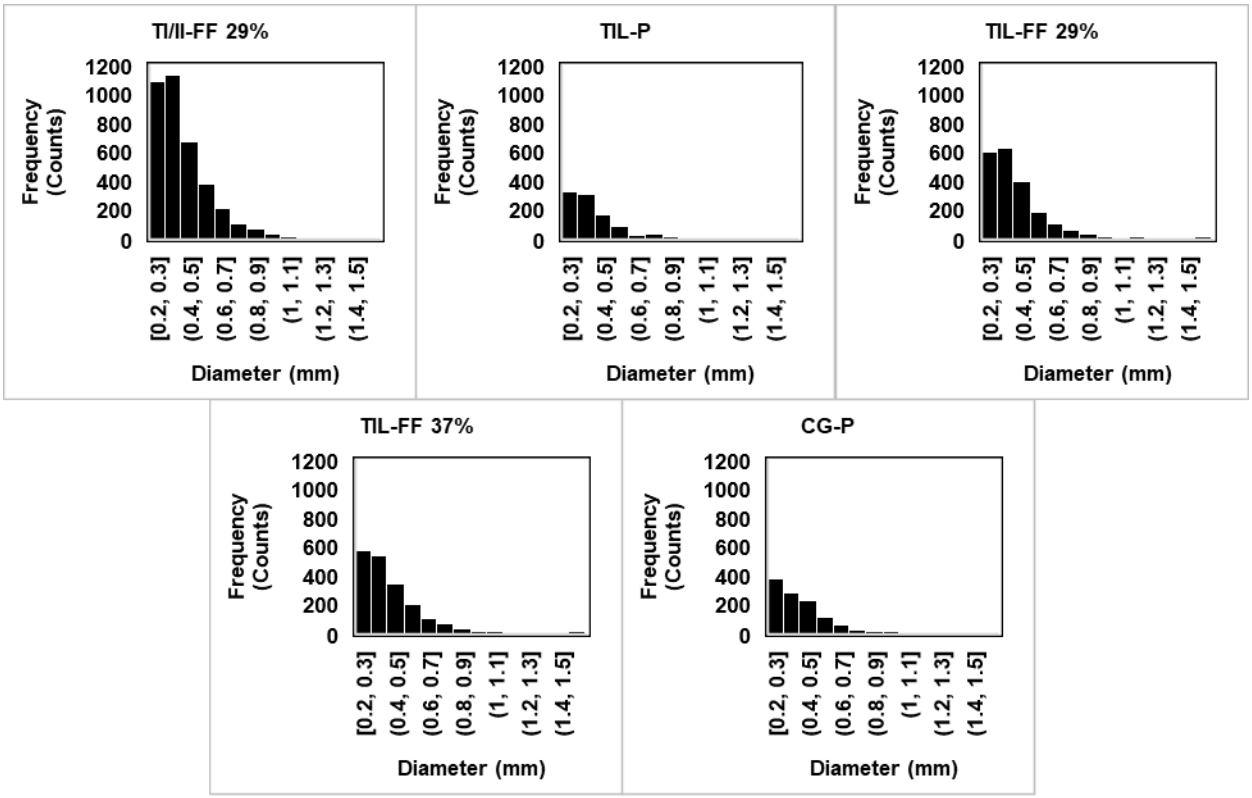

Figure 26: Frequency histograms of cement paste mixtures based on pore diameter (mm)

Naturally, the 28-day electrical resistivity results of TI/II-FF 29% is higher than CG-P. This could be due to a greater degree of discontinuity of the pore system in case of TI/II-FF 29% compared to CG-P. It can be observed from Figure 25 that the number of defects detected (frequency) for TI/II-FF 29% is higher than those of CG-P and TIL-P. This is likely due to a higher degree of hydration in case of TI/II-FF 29% due to a higher fineness of Type I/II portland cement used compared to coarse ground portland cement and Type IL portland limestone cement [65]. A greater degree of hydration will ensure the formation of higher masses of hydration products, e.g., Calcium Silicate Hydrate (C-S-H) and Calcium Hydroxide ($Ca(OH)_2$). These crystals may have a tendency to sub-divide larger void spaces into smaller compartments.

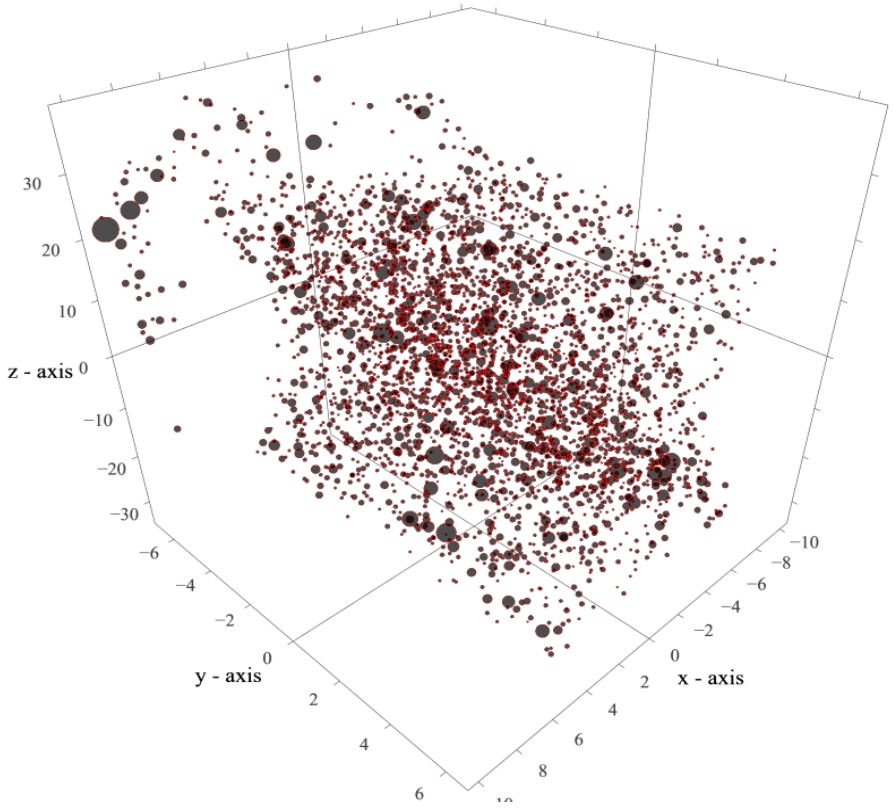

Figure 27: 3D scatter plot of TI/II FF 29% spatial pore size distribution

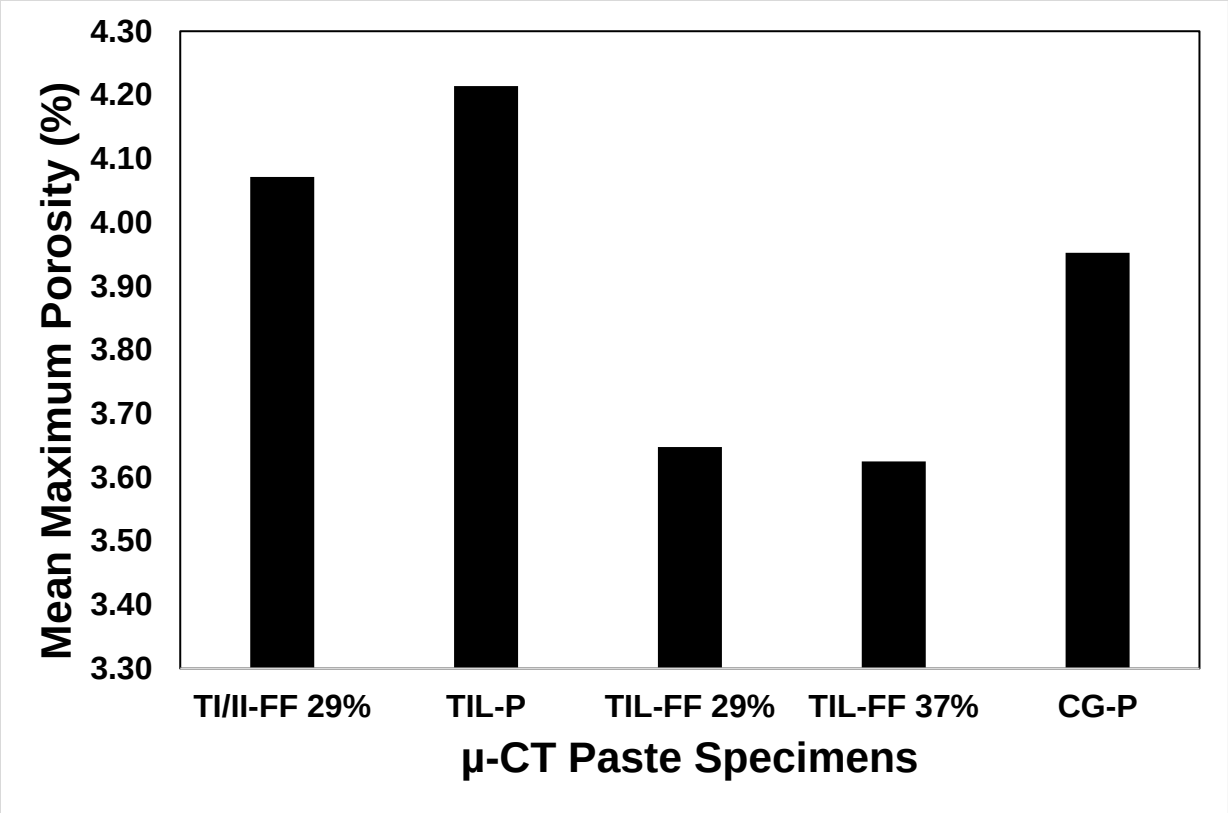

Figure 28: Mean maximum porosity (%) of the paste specimen results under µ-CT

The mixtures containing fly ash may have a higher tendency of void formation due to a likely availability of free water for evaporation [83]. This is mainly because of an un-altered water-cementitious materials ratio. As fly ash is known to impart additional workability to mixtures, such mixtures can be mixed with less water compared to their plain cement counterparts with no supplementary cementitious materials (SCMs) [83]. This may be the reason for higher frequencies of defects seen for the three mixtures containing fly ash (Figure 25).

The distribution of pores in the 3D scatter plot (Figure 27) also reveal that higher porosity zones are slightly higher towards the edges of the samples. This is mainly because of a gradient in relative humidity between different layers of the paste sample. As water recedes faster from the outer layers compared to the core of the sample, the outer layers (near the surface) are drier and therefore more prone to the formation of defects [37,38]. Although not manifested through figures,

the likelihood of obtaining micro-cracks under fluorescence light when observed under a confocal microscope is higher when the slides were processed from the regions of the samples near exposed surfaces.

3.2.2.2. Micro-cracks/Defects (µ-CT) vs. Drying Shrinkage Strain

In this study, paste samples from the five cementitious combinations were cast and subject to drying under restrained conditions. The resultant micro-cracks/Defects results obtained through the µ-CT technique. It may be observed from Figure 28, micro-cracking (as quantified in terms of mean maximum porosity under the hotspots of porosity analysis) for two mixtures containing Type IL cement and fly ash, i.e., TIL-FF 29% and TIL-FF 37% is lower than CG-P and TIL-P. TI/II-FF 29% also had a lower tendency to exhibit micro-cracks than CG-P. It is likely due to an improved microstructure formed by fly ash.

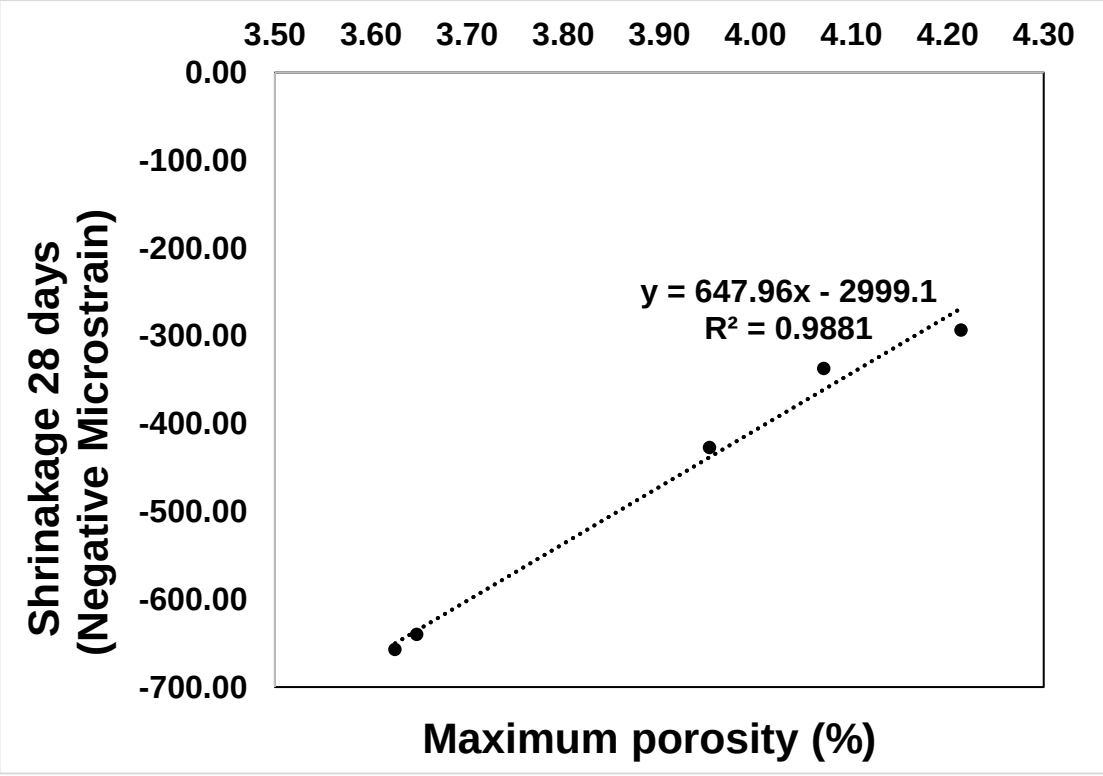

Figure 29: µ-CT vs. shrinkage 28 days scatter plot with a trendline.

Interestingly, similar trends were also seen in the case of 28-day drying shrinkage strain results of concrete containing the mentioned cementitious combinations. As seen in Figure 29, there seems to be a direct proportionality between micro-cracks (%) and 28-day drying shrinkage strain (Negative Microstrain). Table 6 shows a Pearson's correlation test with a 95% confidence interval revealed a coefficient of 0.9 with a P value of < 0.05 (α). This indicates a strong linear correlation between the two parameters. As one of the secondary goals of this work was to investigate potential correlations between microstructure properties of paste and bulk properties of resultant concrete, these results may be indicative of this test methodology being used instead of more laborious, expensive and time-consuming shrinkage test. However, further experimentation and a higher number of samples are needed to investigate the repeatability of this technique and also for statistical significance.

Table 6: Pearson correlation result from Minitab 18.

Correlation: µ-CT, Shrinkage 28 days	
Pearson correlation	0.994
P-value	0.001

3.2.2.3. Defects (µ-CT) vs. Degree of Hydration

The degree of hydration of the cementitious system is a determining factor towards the occurrence of voids and their distribution inside the system [84]. A high rate of formation of C-S-H as indicated by the plateau region of the calorimetry curve will ensure a faster formation of the microstructure. As seen in the case of Figure 10, TIL-P has the highest peak of temperature change among all the five mixtures. Additionally, the nucleation effect of the limestone particle could result in further formation of the hydration products [14]. This, in turn, results in the reduction of defects or voids, as visible in the case of Figure 25. Due to the pozzolanic nature of fly ash, a more

refined microstructure is formed [52]. Bigger voids are likely divided into smaller voids by the secondary hydration products due to fly ash. As a result, voids of all sizes are left in the cementitious system. This is reflected in the void frequency histograms of three mixtures containing fly ash (Figures 25 & 26).

4. OVERALL CONCLUSIONS

In this study, Improved resistance to freeze-thaw deterioration was observed for mixtures containing PLC as compared to other mixtures, Table 7. The following are the key conclusions:

- PLC could help reduce setting times in high fly ash-based mixtures. This is may be due to the rapid hydration and nucleation effect of the additional limestone particles in the mixture.
- OPC mixtures exhibited better free shrinkage in comparison to fly ash mixtures.
- Addition of fly ash to portland limestone cement mixtures seems to have provided better ductility under restrained shrinkage conditions.
- Although the fluorescence microscopy provides more resolution and detail compared to μ-CT, its scope is limited to the slices which are considered to be representative of the overall specimen. There is a chance that the omitted portion of the sample could represent contradicting microstructure results.
- Portland limestone cement with Class F fly ash exhibited similar or slightly better freeze-thaw resistance in comparison to portland cement with Class F fly ash.
- Both μ-CT and FM studies showed that the combination of fly ash and portland limestone cement can be used to reduce the overall mean porosity of the mixture. However, this characteristic might not scale linearly depending upon the dosage of fly ash.

Table 7: Performance matrix

Mix Code	Slump	Air	Unit weight	Final Setting Time	at 28 days: Strength	at 28 days: Split-Tensile Strength	at 28 days: Resistivity	at 28 days: Free Shrinkage	Freeze-Thaw		FM	µ-CT Results	
	(in)	(%)	(lb./ft^3)	(mins)	(psi)	(psi)	(kΩcm)	(x10^{4}strain)	Cycles at 60% P_c	D.F at 60% P_c	Defect %*	Frequency of Pores (counts)	Max Mean Porosity (%)
T I/II FF 29%	4.25	7.6	142.27	343	4322.88	3710	12.50	-337	180	35.96	3.16	3758	4.07
				-	-	-	-	-	-	-	-	-	-
TIL-P	4.00	7.2	141.74	409	4938.31	4042	10.20	-293	204	40.86	3.38	1004	4.21
				-16%	**12%**	**8%**	**-23%**	**15%**	**12%**	**12%**	**-7%**	**274%**	**-3%**
TIL-FF 29%	6.00	7.4	139.27	442	3593.86	3371	9.85	-640	180	35.96	2.83	2119	3.65
				-22%	**-20%**	**-10%**	**-27%**	**-47%**	**0%**	**0%**	**12%**	**77%**	**12%**
TIL-FF 37%	6.00	6.8	141.21	405	3351.29	3344	12.55	-657	180	36.00	1.5	1961	3.63
				-15%	**-29%**	**-11%**	**0%**	**-49%**	**0%**	**0%**	**111%**	**92%**	**12%**
CG-P	5.00	8.0	139.80	467	4470.78	4449	9.25	-427	132	26.45	2.75	1166	3.95
				-27%	**3%**	**17%**	**-35%**	**-21%**	**-36%**	**-36%**	**15%**	**222%**	**3%**

(2nd row of each mix) = Improvement/Dis-improvement percentage in comparison to TI/II-FF 29% (Control) mixture.

FM= Fluorescence Microscopy

Defects %* = micropores + microcracks

P_c – Relative Dynamic Modulus of elasticity

5. FUTURE RESEARCH RECOMMENDATIONS

- Altering W/C ratio

Altering W/C ratio could help to achieve better freeze-thaw resistance as well as optimize the mixture for higher strength, since fly ash improves workability and requires marginally less water to achieve the same consistency and performance as compared to OPC, the amount of free-water is increased in the presence of high amounts of fly ash. Thus, reducing the water from the mixture can help mitigate the free water and help produce a better, more sound concrete which may lead to lower permeability and better freeze-thaw resistance.

- Statistical analysis of the micro-structure results

To make a better correlation between mechanical properties (calorimetry, resistivity and shrinkage) and the results from microstructure study, the number of specimens needs to increase to potentially create a statistical model and show better statistical significance values. Thus, leading to new findings and a better understanding of effects like permeability and micro-defects on other mechanical properties and also quicker and streamlined testing methods.

- Better representative slices in case of fluorescence microscopy

Developing an in-house microstructure study workflow starting from the creation and polishing the of the specimen slices for fluorescence microscopy can be beneficial leading to more accurate results. In this study, a petrographer was used to create the slices, which meant the plane selected for the creation the thin slices, may or may not be representative of the overall specimen. More control over this process would provide new opportunities like fine-tuning the representative plane depending on other microstructure study techniques like µ-CT and a higher number of slices.

REFERENCES

[1] T.C. Powers, Structure and Physical Properties of Hardened Portland Cement Paste, J. Am. Ceram. Soc. 41 (1958) 1–6. doi:10.1111/j.1151-2916.1958.tb13494.x.

[2] H.S. Shang, W.Q. Cao, B. Wang, Effect of fast freeze-thaw cycles on mechanical properties of ordinary-air-entrained concrete, Sci. World J. 2014 (2014). doi:10.1155/2014/923032.

[3] S.W. Tang, Y. Yao, C. Andrade, Z.J. Li, Recent durability studies on concrete structure, Cem. Concr. Res. 78 (2015) 143–154. doi:10.1016/J.CEMCONRES.2015.05.021.

[4] P.K. Mehta, P.J.M. Monteiro, Concrete: Microstructure, Properties, and Materials, 4th ed., McGraw-Hill Education, 2013.

[5] T. Cavalline, M.T. Ley, L.L. Sutter, W.J. Weiss, A Road Map for Research and Implementation of Freeze-Thaw Resistant Highway Concrete Resistivity, Formation Factor and Transport View project Concrete Patching Materials and Techniques and Guidelines for Hot Weather Concreting View project, 2016. https://www.researchgate.net/publication/307536732.

[6] S. H.Kosmatka, M. L.wilson, Design and Control of Concrete Mixtures, 2011. http://www.cement.org/bookstore/supporting/cd100/EB001Frt.pdf.

[7] V. Penttala, Surface and internal deterioration of concrete due to saline and non-saline freeze-thaw loads, Cem. Concr. Res. 36 (2006) 921–928. doi:10.1016/j.cemconres.2005.10.007.

[8] P.D. Tennis, M.D.A. Thomas, W.J. Weiss, State-of-the-Art Report on Use of Limestone in Cements at Levels of up to 15 %, Portl. Cem. Assoc. (2011) 1–78. http://www.cptechcenter.org/ncc/documents/SN3148_Use of Limestone in Cements.pdf.

[9] V.T. Cost, G. Knight, W. Wilson, J. Shannon, I.L. Howard, Performance of Typical Concrete Mixtures for Transportation Structures as Influenced by Portland-Limestone Cements from Five Sources, Int. Concr. Sustain. Conf. (2013) 1–11.

[10] H. Sun, B. Fan, S.A. Memon, Z. Cen, X. Gao, B. Lin, B. Liu, D. Li, F. Xing, X. Zhang, 3D particle size distribution of inter-ground Portland limestone/slag cement from 2D observations: Characterization and distribution evaluation, Constr. Build. Mater. 147 (2017) 550–557. doi:10.1016/j.conbuildmat.2017.04.070.

[11] M.D.. Thomas, D. Hooton, K. Cail, B.. Smith, J. De Wal, K.G. Kazanis, Field Trials of Concretes Produced with Portland Limestone Cement, Concr. Int. 35 (2010) 35–41. https://pdfs.semanticscholar.org/d0fd/3ea8f35a664c1c14cfc0c540bffd2cf22a53.pdf.

[12] T. Barrett, H. Sun, T. Nantung, W. Weiss, Performance of Portland Limestone Cements, Transp. Res. Rec. J. Transp. Res. Board. 2441 (2014) 112–120. doi:10.3141/2441-15.

[13] S. Tsivilis, N. Voglis, J. Photou, Study on the intergrinding of clinker and limestone, Miner. Eng. 12 (1999) 837–840. doi:10.1016/S0892-6875(99)00068-0.

[14] V. Bonavetti, H. Donza, G. Menéndez, O. Cabrera, E.F. Irassar, Limestone filler cement in low w/c concrete: A rational use of energy, Cem. Concr. Res. 33 (2003) 865–871. doi:10.1016/S0008-8846(02)01087-6.

[15] T. Matschei, B. Lothenbach, F.P. Glasser, The role of calcium carbonate in cement hydration, Cem. Concr. Res. 37 (2007) 551–558. doi:10.1016/j.cemconres.2006.10.013.

[16] V.L. Bonavetti, V.F. Rahhal, E.F. Irassar, Studies on the carboaluminate formation in limestone filler-blended cements, Cem. Concr. Res. 31 (2001) 853–859. doi:10.1016/S0008-8846(01)00491-4.

[17] W.A. Klemm ', L.D. Adams ', An Investigation of the Formation of Carboaluminates, Am. Soc. Test. Mater. Philadelphia. ASTMSTP 10 (1990) 60–72. doi:10.1520/STP23472S.

[18] A.M. Ramezanianpour, R.D. Hooton, A study on hydration, compressive strength, and porosity of Portland-limestone cement mixes containing SCMs, Cem. Concr. Compos. 51 (2014) 1–13. doi:10.1016/j.cemconcomp.2014.03.006.

[19] N. Voglis, G. Kakali, E. Chaniotakis, S. Tsivilis, Portland-limestone cements. Their properties and hydration compared to those of other composite cements, Cem. Concr. Compos. 27 (2005) 191–196. doi:10.1016/j.cemconcomp.2004.02.006.

[20] A.A. Ramezanianpour, E. Ghiasvand, I. Nickseresht, M. Mahdikhani, F. Moodi, Influence of various amounts of limestone powder on performance of Portland limestone cement concretes, Cem. Concr. Compos. 31 (2009) 715–720.

[21] R.K. Dhir, M.C. Limbachiya, M.J. McCarthy, A. Chaipanich, Evaluation of Portland limestone cements for use in concrete construction, Mater. Struct. 40 (2007) 459–473. doi:10.1617/s11527-006-9143-7.

[22] E.F. Irassar, V.L. Bonavetti, G. Menendez, H. Donza, O. Cabrera, Mechanical properties and durability of concrete made with portland limestone cement, ACI Spec. Publ. 202 (2001) 431–450.

[23] V. Bonavetti, H. Donza, V. Rahhal, E.F. Irassar, High-strength concrete with limestone filler cements, ACI Spec. Publ. 186 (1999) 567–580.

[24] V.M. Malhotra, Durability of concrete incorporating high-volume of low-calcium (ASTM Class F) fly ash, Cem. Concr. Compos. 12 (1990) 271–277. doi:10.1016/0958-9465(90)90006-J.

[25] B. Lothenbach, K. Scrivener, R.D. Hooton, Supplementary cementitious materials, Cem. Concr. Res. 41 (2011) 1244–1256. doi:10.1016/j.cemconres.2010.12.001.

[26] D.P. Bentz, Blending different fineness cements to engineer the properties of cement-based materials, Mag. Concr. Res. 62 (2010) 327–338. doi:10.1680/macr.2008.62.5.327.

[27] T. Barrett, H. Sun, C. Villani, L. Barcelo, J. Weiss, Early-Age Shrinkage Behavior of Portland Limestone Cement Pore size distribution trumps fineness, Concr. Int. 32 (2014) 51–57. https://www.concrete.org/publications/internationalconcreteabstractsportal.aspx?m=details&i=51686601.

[28] B. Yilmaz, A. Olgun, Studies on cement and mortar containing low-calcium fly ash, limestone, and dolomitic limestone, Cem. Concr. Compos. 30 (2008) 194–201. doi:10.1016/j.cemconcomp.2007.07.002.

[29] C.D. Medlin, Durability of pavement concrete with replacement of cement by flyash and portland limestone cement, ProQuest Dissertations Publishing, 2016. https://search.proquest.com/docview/1842666817?pq-origsite=gscholar.

[30] B.W. Langan, R.C. Joshi, M.A. Ward, Strength and durability of concretes containing 50% Portland cement replacement by fly ash and other materials, Can. J. Civ. Eng. 17 (1990) 19–27. doi:10.1139/l90-004.

[31] A.P. Barker and Matthews, J. D., Concrete Durability Specification by Water/Cement or Compressive Strength for European Cement Types, ACI Spec. Publ. SP145-62 (1994) 1135 to 1160.

[32] J. Matthews, Performance of Limestone Filler Cement Concrete, Euro-Cements – Impact ENV 197 Concr. Constr. (Ed.), E&FN Spon, London, Pp. 113-147. 197 (1994) 113–147.

[33] P.D. Tennis, M.D.A. Thomas, W.J. Weiss, State-of-the-Art Report on Use of Limestone in Cements at Levels of up to 15 %, Portl. Cem. Assoc. (2011) 1–78. https://pdfs.semanticscholar.org/6545/02baaf8abac3911b60829bb9d2264fbbd707.pdf (accessed February 12, 2018).

[34] R.D. Hooton, A. Ramezanianpour, U. Schutz, Decreasing the Clinker Component Materials: Performance of Portland-Limestone Cements in Concrete in combination with Supplementary Cementing Materials, Concr. Sustain. Conf. (2010) 1–15. https://www.nrmca.org/ctf/2010cscproceedings/documents/Hooton Paper 4-14-10.pdf (accessed February 12, 2018).

[35] North Dakota. Department of Transportation., Standard Specifications for Road and Bridge Construction, Bismarck, N.D. : North Dakota Dept. of Transportation, 2014. http://www.dot.nd.gov/divisions/environmental/docs/supspecs/2014StandardSpecifications.pdf.

[36] P. Taylor, X. Wang, Concrete Pavement Mixture Design and Analysis (MDA): Factors Influencing Drying Shrinkage, 2014. http://lib.dr.iastate.edu/intrans_reports%5Cnhttp://lib.dr.iastate.edu/intrans_reports/75.

[37] J. Bisschop, J.G.M. Van Mier, Drying Shrinkage Microcracking in Cement-based Materials, Heron, 47 (3), 2002. (2002). https://www.narcis.nl/publication/RecordID/oai:tudelft.nl:uuid:6a2bc507-02ae-4077-9d50-7e348045d381.

[38] C. de Sa, F. Benboudjema, M. Thiery, J. Sicard, Analysis of microcracking induced by differential drying shrinkage, Cem. Concr. Compos. 30 (2008) 947–956. doi:10.1016/j.cemconcomp.2008.06.015.

[39] H. Samouh, E. Rozière, A. Loukili, Drying depth and size effect on long-term behavior of concrete, Key Eng. Mater. 711 (2016) 645–651. doi:10.1617/s11527-015-0771-7.

[40] P. Mohr, W. Hansen, E. Jensen, I. Pane, Transport properties of concrete pavements with excellent long-term in-service performance, Cem. Concr. Res. 30 (2000) 1903–1910. doi:10.1016/S0008-8846(00)00452-X.

[41] H. Yasarer, Y.M. Najjar, Characterizing the Permeability of Kansas Concrete Mixes Used in PCC Pavements, Int. J. Geomech. 14 (2014) 04014017. doi:10.1061/(ASCE)GM.1943-5622.0000362.

[42] A.. Neville, Properties of concrete, 5th Editio, Pitman Books, Great Britain, 2012.

[43] ASTM Standard C1581 - 18a, Standard Test Method for Determining Age at Cracking and Induced Tensile Stress Characteristics of Mortar and Concrete under Restrained Shrinkage, ASTM International, Conshohocken, PA, 2018. doi:10.1520/C1581_C1581M-18A.

[44] ASTM Standard C856 - 18a, Standard Practice for Petrographic Examination of Hardened Concrete, ASTM International, Conshohocken, PA, 2018. doi:10.1520/C0856-18A.

[45] S. Mindess, S. Diamond, A preliminary SEM study of crack propagation in mortar, Cem. Concr. Res. 10 (1980) 509–519. doi:10.1016/0008-8846(80)90095-2.

[46] A. Rashed, R.B. Williamson, Microstructure of entrained air voids in concrete, J. Mater. Res. 6 (1991) 2004–2012. doi:DOI: 10.1557/JMR.1991.2004.

[47] R. Zerbino, G. Giaccio, S. Marfil, Evaluation of alkali-silica reaction in concretes with natural rice husk ash using optical microscopy, Constr. Build. Mater. 71 (2014) 132–140. doi:10.1016/j.conbuildmat.2014.08.022.

[48] I. Tekin, R. Birgul, I. Ozgur Yaman, O. Gencel, H. Yilmaz Aruntas, Monitoring macro voids in mortars by computerized tomography method, Meas. J. Int. Meas. Confed. 63 (2015) 299–308. doi:10.1016/j.measurement.2014.11.034.

[49] H.S. Wong, A.M. Pappas, R.W. Zimmerman, N.R. Buenfeld, Effect of entrained air voids on the microstructure and mass transport properties of concrete, Cem. Concr. Res. 41 (2011) 1067–1077. doi:10.1016/j.cemconres.2011.06.013.

[50] H.S. Wong, N.R. Buenfeld, Patch microstructure in cement-based materials: Fact or artefact?, Cem. Concr. Res. 36 (2006) 990–997. doi:10.1016/j.cemconres.2006.02.008.

[51] P.K. Mehta, P.J.M. Monteiro, Concrete: microstructure, properties, and materials, McGraw-Hill Education, 2006. doi:10.1036/0071462899.

[52] Q. Zeng, K. Li, T. Fen-Chong, P. Dangla, Pore structure characterization of cement pastes blended with high-volume fly-ash, Cem. Concr. Res. 42 (2012) 194–204. doi:10.1016/j.cemconres.2011.09.012.

[53] R.M. Lawrence, T.J. Mays, S.P. Rigby, P. Walker, D. D'Ayala, Effects of carbonation on the pore structure of non-hydraulic lime mortars, Cem. Concr. Res. 37 (2007) 1059–1069. doi:10.1016/j.cemconres.2007.04.011.

[54] M. Arandigoyen, J.I. Alvarez, Pore structure and mechanical properties of cement–lime mortars, Cem. Concr. Res. 37 (2007) 767–775.

[55] X. Wang, P. Taylor, K. Wang, M. Lim, Monitoring of setting time of self-consolidating concrete using ultrasonic wave propagation method and other tools, Mag. Concr. Res. 68 (2016) 151–162. doi:10.1680/macr.15.00076.

[56] ASTM Standard C305-14, Designation: C305 − 14 Standard Practice for Mechanical Mixing of Hydraulic Cement Pastes and Mortars of Plastic Consistency, ASTM Int. (n.d.). doi:10.1520/C0305-14.

[57] A. du Plessis, B.J. Olawuyi, W.P. Boshoff, S.G. le Roux, Simple and fast porosity analysis of concrete using X-ray computed tomography, Mater. Struct. 49 (2016) 553–562. doi:10.1617/s11527-014-0519-9.

[58] J.F. Best, R.O. Lane, Testing for Optimum Pumpability of Concrete, Concr. Int. 2 (1980) 9–17.

[59] C.H. Huang, S.K. Lin, C.S. Chang, H.J. Chen, Mix proportions and mechanical properties of concrete containing very high-volume of Class F fly ash, Constr. Build. Mater. 46 (2013) 71–78. doi:10.1016/j.conbuildmat.2013.04.016.

[60] E.H. Kadri, S. Aggoun, G. De Schutter, K. Ezziane, Combined effect of chemical nature and fineness of mineral powders on Portland cement hydration, Mater. Struct. 43 (2010) 665–673. doi:10.1617/s11527-009-9519-6.

[61] K. De Weerdt, M. Ben Haha, G. Le Saout, K.O. Kjellsen, H. Justnes, B. Lothenbach, Hydration mechanisms of ternary Portland cements containing limestone powder and fly ash, Cem. Concr. Res. 41 (2011) 279–291. doi:10.1016/j.cemconres.2010.11.014.

[62] J. Shannon, I.L. Howard, V. Tim Cost, R. Shannon, T. Cost, Potential of Portland-Limestone Cement to Improve Performance of Concrete Made With High Slag Cement and Fly Ash Replacement Rates " Potential of Portland-Limestone Cement to Improve Performance of Concrete Made With High Slag Cement and Fly Ash Repl, J. Test. Eval. 45 (2017) 873–889. doi:10.1520/JTE20150306.

[63] L. Gurney, D. Bentz, T. Sato, W. Weiss, Reducing Set Retardation in High-Volume Fly Ash Mixtures with the Use of Limestone, Transp. Res. Rec. J. Transp. Res. Board. 2290 (2012) 139–146. doi:10.3141/2290-18.

[64] G. Kakali, S. Tsivilis, E. Aggeli, M. Bati, Hydration products of C3A, C3S and Portland cement in the presence of CaCO3, Cem. Concr. Res. 30 (2000) 1073–1077. doi:10.1016/S0008-8846(00)00292-1.

[65] D.P. Bentz, E.J. Garboczi, C.J. Haecker, O.M. Jensen, Effects of cement particle size distribution on performance properties of Portland cement-based materials, Cem. Concr. Res. 29 (1999) 1663–1671. doi:10.1016/S0008-8846(99)00163-5.

[66] K.L. Scrivener, P. Juilland, P.J.M. Monteiro, Advances in understanding hydration of Portland cement, Cem. Concr. Res. 78 (2015) 38–56. doi:10.1016/j.cemconres.2015.05.025.

[67] M.D.A. Thomas, Optimizing the Use of Fly Ash in Concrete, Portl. Cem. Assoc. (2007) 24. doi:10.15680/IJIRSET.2015.0409047.

[68] I. De La Varga, J. Castro, D. Bentz, J. Weiss, Application of internal curing for mixtures containing high volumes of fly ash, Cem. Concr. Compos. 34 (2012) 1001–1008. doi:10.1016/j.cemconcomp.2012.06.008.

[69] R. Siddique, Performance characteristics of high-volume Class F fly ash concrete, Cem. Concr. Res. 34 (2004) 487–493. doi:10.1016/j.cemconres.2003.09.002.

[70] G.M. Giaccio, V.M. Malhotra, Concrete Incorporating High Volumes of ASTM Class F Fly Ash, CCAGDP. 10 (1988) 88–95. https://compass.astm.org/download/CCA10088J.24481.pdf (accessed March 19, 2018).

[71] R. Detwiler, P.D. Tennis, The Use of Limestone in Portland Cement : A State-of-the-Art Review, Portl. Cem. Assoc. (2003) 1–38. http://cement.org/astmc01/eb227.pdf.

[72] R. Polder, C. Andrade, B. Elsener, Ø. Vennesland, J. Gulikers, R. Weidert, M. Raupach, Test methods for on site measurement of resistivity of concrete, Mater. Struct. 33 (2000) 603–611. doi:10.1007/BF02480599.

[73] T. Ayub, S.U. Khan, F.A. Memon, Mechanical characteristics of hardened concrete with different mineral admixtures: A review, Sci. World J. 2014 (2014). doi:10.1155/2014/875082.

[74] D.P. Bentz, E.J. Garboczi, C.J. Haecker, O.M. Jensen, Effects of cement particle size distribution on performance properties of Portland cement-based materials, Cem. Concr. Res. 29 (1999) 1663–1671. https://ac.els-cdn.com/S0008884699001635/1-s2.0-S0008884699001635-main.pdf?_tid=770577ab-c4f6-4202-a919-6f0f676629a5&acdnat=1524458995_9d0566b54df6d17209a0a7e412e883a1.

[75] J. Weiss, P. Lura, F. Rajabipour, G. Sant, Performance of shrinkage redcution admixture at different humidities and at early ages, ACI Materails J. 105 (2008) 478–486. doi:10.1007/s13398-014-0173-7.2.

[76] T. Barrett, H. Sun, C. Villani, L. Barcelo, J. Weiss, Early-age shrinkage behavior of Portland limestone cement, Concr. Int. 36 (2014).

[77] J.G.L. Munday, L.T. Ong, L.B. Wong, R.K. Dhir, Load independent movements in opc/pfa concrete, in: Proceedings, Int. Symp. Use PFA Concr., 1982: pp. 243–246.

[78] L.. Jiang, V.. Malhotra, Reduction in water demand of non-air-entrained concrete incorporating large volumes of fly ash, Cem. Concr. Res. 30 (2000) 1785–1789. doi:10.1016/S0008-8846(00)00397-5.

[79] P. Kumar Mehta, High-performance, high-volume fly ash concrete for sustainable development, Int. Work. Sustain. Dev. Concr. Technol. (2004) 3–14. doi:10.15680/IJIRSET.2015.0409047.

[80] P. Pipilikaki, M. Beazi-Katsioti, The assessment of porosity and pore size distribution of limestone Portland cement pastes, Constr. Build. Mater. 23 (2009) 1966–1970. doi:10.1016/j.conbuildmat.2008.08.028.

[81] S. Tsivilis, G. Batis, E. Chaniotakis, G. Grigoriadis, D. Theodossis, Properties and behavior of limestone cement concrete and mortar, Cem. Concr. Res. 30 (2000) 1679–1683. doi:10.1016/S0008-8846(00)00372-0.

[82] G. Quercia, P. Spiesz, G. Hüsken, H.J.H. Brouwers, SCC modification by use of amorphous nano-silica, Cem. Concr. Compos. 45 (2014) 69–81. doi:10.1016/j.cemconcomp.2013.09.001.

[83] L.. Jiang, V.. Malhotra, Reduction in water demand of non-air-entrained concrete incorporating large volumes of fly ash, 2000. doi:10.1016/S0008-8846(00)00397-5.

[84] I. Odler, M. Rößler, Investigations on the relationship between porosity, structure and strength of hydrated Portland cement pastes. II. Effect of pore structure and of degree of hydration, Cem. Concr. Res. 15 (1985) 401–410. doi:10.1016/0008-8846(85)90113-9.

[85] P.A. and W.W. Sucaet Yves, Free Whole Slide Image Viewer – PMA.Start | Universal Digital Microscopy Software, (n.d.). https://free.pathomation.com/.